



# UNIVERSITÀ DELLA CALABRIA

Dipartimento di Ingegneria Informatica,  
Modellistica, Elettronica e Sistemistica

Dottorato di Ricerca in Scienze, Comunicazione  
e Tecnologie  
**XXVIII ciclo**

*Tesi di Dottorato*

## PERMITTIVITY CHARACTERIZATION OF A DIELECTRIC MATERIAL USING RADAR TECHNIQUES

Paul David Moreno Aviles

DIMES  
Novembre 2015

Settore Scientifico Disciplinare: ING-INF/02

**UNIVERSITA' DELLA CALABRIA**

Dipartimento di Ingegneria Informatica, Modellistica, Elettronica e Sistemistica

**Dottorato di Ricerca in**

Scienze, Comunicazione e Tecnologie

**CICLO**

XXVIII

**Permittivity Characterization of a Dielectric Material using Radar Techniques****Settore Scientifico Disciplinare ING-INF/02**

**Coordinatore:** Ch.mo Prof. Pietro Pantano  
Firma Pietro Pantano

**Supervisore:** Ch.mo Prof. Felice Crupi  
Firma Felice Crupi

**Correlatori:** Ch.mo Prof. Giuseppe Di Massa  
Firma G. Di Massa

Ch.mo Prof.ssa Sandra Costanzo  
Firma Sandra Costanzo

**Dottorando:** Dott. Paul David Moreno Avilés  
Firma Paul David Moreno Avilés

to my parents, for their love, support and courage.



---

## Acknowledgement

I give thanks for this Phd mainly to God for allowing me to live with intensity, sacrifice dedication and responsibility these three years of hard work, which for me these were the most intellectual and academic years of my life without leaving behind harvested and learned values.

A special thanks to my brother Hugo, who with his wife Ximena and his sweet daughter Sofia were the persons who welcomed me during my early days in Italy, they guided me and assisted me in the transition from one country to another making it more easy to endure.

To Felice Crupi for being my thesis supervisor and be the person who brokered so that I could come and make my PHD studies at the University of Calabria.

Thankful to Professor Giuseppe Di Massa and Professor Sandra Costanzo, my co-tutors, who they together proposed my research and have contributed significantly to the development of this, they have given me their full support and knowledge in order to this thesis can be performed.

I would also like to thank the team of  $\mu$ wavelab Laboratory of the University of Calabria UNICAL, especially "the Antonios": Antonio Borgia, Antonio Costanzo and Antonio Raffo, with whom we have formed a beautiful friendship and with whom we have been able to maintain technical talks, social and others, making more comfortable the surroundings in the lab.

An infinite gratitude to my family: my parents Hugo and Julia, whose great wisdom has been able to give me the necessary support and encouragement in the most difficult moments of my stay; my sisters and brothers: July, Susy, Huguito and Isra, which equally with their husbands, wives and children have filled me with love and tenderness in a way that only they can do it.

## VIII Acknowledgement

I could not forget to thank my friends from Ecuador who in one way or another have always been present, either with a message of support or with an occasional joke to brighten the days, please remain friends after so long.

I also thank each and every one of the people i met here, undoubtedly they earned my heart, my admiration and friendship, i understood that every person leaves a teaching and an experience different and unforgettable.

Finally a great and extensive thanks to the Ecuadorian community in the University of Calabria, without them this great journey and this great achievement would not have been the same, thanks for all the known places, the experiences and knowledge gained.

*Sincerely*

*David*

---

## Preface

This doctoral thesis work has the results of three years of research (2013 - 2016) developed in the  $\mu$ wavelab laboratory of the University of Calabria in the "DIPARTIMENTO DI INGEGNERIA, INFORMATICA, MODELLISTICA E SISTEMISTICA" DIMES.

The work has been started with the habituation of research done in the  $\mu$ wavelab laboratory, always with the supervision of professor Felice Crupi and the counselling of my co-tutors Giuseppe Di Massa and Sandra Costanzo, with this, a period of study, reading and data collection about SDRadar (Software Defined Radar) was begun.

Later, with my supervisors the theme of thesis was selected, and it was chosen the "PERMITTIVITY CHARACTERIZATION OF A DIELECTRIC MATERIAL USING RADAR TECHNIQUES", since today the methods of characterization or permittivity measurements are highly expensive and a lot of the research centres do not have the resources to carry out this work.

For this reason this theme of thesis was proposed, because the dielectric material characterization becomes an important tool for the construction of antennas, transmission lines, wave guides and electronic devices such as capacitors or inductors; and the possibility of each laboratory can make this measurements inside of their own installations using materials and equipment low cost obtaining optimal results is the principal motivation for this doctoral thesis.

The starting point of this work was the signal generation to be processed in a SDRadar environment, special interest was taken in OFDM (Orthogonal Frequency Division Multiplexing) signals and FMCW (Frequency Modulation Continuous Wave) signals, with these, previous works was recreated in order to understand the research line and the objectives of this.

At the beginning the NI USRP - 2920 card from National Instruments and property of the  $\mu$ wavelab laboratory was used to make the first tests with SDRadar technology. The card generates the signals, then these were transmitted, received and processed, obtaining the related data concerning to

target detection and some characteristics of it such as movement, velocity and direction.

Unfortunately, the NI USRP - 2920 card does not provide the resolution necessary for characterize a dielectric material sample that usually it has thickness dimensions very small. This is because the bandwidth generated by the card is only of 500 MHz. For this reason, it is chosen as signal generator an Anritsu Vector network Analyser VNA, it provides a bandwidth of 8 GHz. generating a resolution of 1.7mm.

The next step in the research was to develop the mathematical models in base at the disposition and the configuration of the system, for this, several months were employed, in which were applied hard work and the analysis of physic concepts involved in system behaviour. First, the mathematical model for real permittivity was obtained, this allowed to make simulations and measurements, then, the model for complex permittivity was developed, this means that it is possible to calculate the real part of permittivity and the imaginary part of this magnitude.

Finally, for validate these models, Matlab scripts were realized, firstly to simulate the behaviour of the operation system and later to process the obtained data with measures done by the implemented system.

The results obtained in the simulations were compared with those obtained in the measurements, and these in turn with materials which permittivity is known whose values are exposed in literature.

Rende (Cosenza),

*Paúl David Moreno Avilés*

Noviembre 2015



---

## Prefazione

Il presente Lavoro di tesi dottorale contiene i risultati di tre anni di ricerca (2013-2016) svolti nel laboratorio  $\mu$ wavelab della Università della Calabria, presso il "DIPARTIMENTO DI INGEGNERIA, INFORMATICA, MODELLISTICA E SISTEMISTICA" DIMES.

Il Lavoro iniziato facendo conoscenza della ricerca in atto effettuata nel laboratorio wavelab, esso diede inizio ad un periodo di studio, lettura e raccolta di informazioni riguardante a SDRadar (Software Dened Radar) tutto ciò è stato possibile grazie alla collaborazione e supervisione del Professore Felice Crupi e il consiglio dei miei correlatori Professore Giuseppe Di Massa e la Professoressa Sandra Costanzo.

Insieme ai miei tutor è stato scelto il titolo della ricerca denominata: "Caratterizzazione Complessa di un materiale Dielettrico usando tecniche SDRadar", Attualmente però i metodi per fare la caratterizzazione o la misurazione della permittività hanno costi elevati e molti centri di ricerca non sono attrezzati per la realizzazione di tale lavoro.

Per tale motivo, si è proposto questo tema di ricerca che rappresenta uno strumento importantissimo per la fabbricazione di antenne, linee di trasmissione, guide di onda e dispositivi elettronici come condensatori o induttori, ottenendo quindi come vantaggio quello di poter realizzare tali lavori all'interno dello stesso laboratorio con materiali e attrezzature di basso costo e con ottimi risultati pertanto esso diventa il punto centrale della tesi dottorale.

Il punto iniziale di questa ricerca è stata quella creare dei segnali per essere elaborati all'interno di un ambiente SDRadar, soprattutto focalizzandosi nei segnali OFDM (Orthogonal Frequency Division Multiplexing) e FMCW (Frequency Modulation Continuous Wave), con le quali si ricreano degli studi precedenti al fine di comprendere la linea di lavoro sulla quale tale ricerca si sarebbe svolta.

Inizialmente è stata utilizzata la scheda NI USRP - 2920 della National Instruments (propriet del laboratorio  $\mu$ wavelab), per realizzare i primi test con tecnologia SDRadar, con cui si generavano dei segnali corrispondenti, dove vengono trasmessi, ricevuti e processati, con lo scopo di ottenere dei dati

di rilevamento di un target avente come caratteristiche: movimento, velocità e direzione.

Purtroppo con la scheda NI USRP - 2920 non si otteneva la risoluzione desiderata per caratterizzare un campione di materiale dielettrico, che di solito ha le dimensioni di spessore più ridotte, ciò è dovuto alla banda che genera la scheda di solo 500 MHz. Per questa ragione si è optato di scegliere come generatore dei segnali un VNA Vector Network Analyzer di marca Anritsu che genera una banda fino 8 GHz. provvedendo una risoluzione di 1.7mm.

Il passo successivo fu quello di sviluppare i modelli matematici in base alla disposizione e la configurazione del sistema pianificato, per effettuare questo ci sono voluti diversi mesi di duro lavoro e analisi dei concetti fisici che intervengono nel comportamento del sistema. Inizialmente è stato ottenuto il modello matematico per il calcolo della parte reale della permittività dopo aver effettuate delle simulazioni, misure e i test pertinenti, si sviluppò il modello per il calcolo della complessa permittività, questo vuol dire ,calcolare tanto il valore reale come il valore immaginario di questa portata.

In conclusione quindi per rendere validi questi modelli ottenuti, sono stati fatti alcuni script in Matlab, prima per poter simulare il comportamento del sistema di fronte a un campione di dielettrico e poi per processare i dati ottenuti con le misure del sistema implementato.

I risultati delle simulazioni sono stati poi confrontati con quelli ottenuti nelle misure e questi alla loro volta confrontati con i valori dei materiali conosciuti e presenti in letteratura.

Rende (Cosenza),

*Paúl David Moreno Avilés*

Noviembre 2015

---

## Prefacio

Este trabajo de tesis doctoral contiene los resultados de tres años de investigación (2013 - 2016) desarrollados en el laboratorio  $\mu$ wavelab de la Universidad de la Calabria, en el "DIPARTIMENTO DI INGEGNERIA, INFORMATICA, MODELLISTICA E SISTEMISTICA" DIMES.

El trabajo se inició con la familiarización de la investigación que se realiza en el laboratorio  $\mu$ wavelab, siempre con la tutela y supervisión del profesor Felice Crupi y el asesoramiento de mis co-tutores Giuseppe Di Massa y Sandra Costanzo, con lo cual un período de estudio, lectura y recolección de información correspondiente a SDRadar (Software Defined Radar) dio inicio.

Posteriormente junto con mis tutores se decidió el tema de investigación a ser desarrollado y se optó por la "Caracterización Compleja de un material Dieléctrico utilizando técnicas SDRadar", ya que en la actualidad los métodos de caracterización o medición de la permitividad son elevadamente costosos y muchos de los centros de investigación no cuentan con dichos recursos para la realización de esta labor.

Por esta razón se ha propuesto este tema de investigación ya que la caracterización de un material dieléctrico se convierte en una herramienta importantísima para la construcción de antenas, líneas de transmisión, guías de onda y dispositivos electrónicos como capacitores o inductores; y el poder realizar esta medición dentro del mismo laboratorio con materiales y equipos de bajo coste obteniendo resultados idóneos, se convierte en la motivación principal de este tema de tesis doctoral.

El punto inicial de desarrollo fue la generación de señales para ser procesadas en un entorno de SDRadar, con lo cual se puso especial énfasis en las señales OFDM (Orthogonal Frequency Division Multiplexing) y FMCW (Frequency Modulation Continuous Wave), con las cuales inicialmente se recrearon trabajos precedentes con el fin de entender completamente la línea de trabajo en la cual se desarrollaría esta investigación.

En principio se utilizó la tarjeta NI USRP - 2920 de la National Instruments propiedad del laboratorio  $\mu$ wavelab, para realizar las primeras pruebas con tecnología SDRadar, con la cual se generaba las señales correspondientes,

luego estas eran transmitidas, recibidas y procesadas obteniendo los datos respectivos de detección de un objeto y algunas características como movimiento velocidad y dirección.

Lastimosamente la tarjeta NI USRP - 2920 no proveía la resolución necesaria para caracterizar una muestra de material dieléctrico que generalmente tiene dimensiones de espesor más reducidas, esto debido a la banda que genera el dispositivo de solo 500 MHz. Por lo cual se optó por elegir como generador de señales un VNA Vector Network Analyzer de marca Anritsu que provee una banda de hasta 8 GHz. lo cual genera una resolución de 1.7 mm.

El siguiente paso en la investigación fue desarrollar los respectivos modelos matemáticos en base a la disposición y la configuración del sistema planificado, lo cual conllevó varios meses de arduo trabajo y análisis de los conceptos físicos que intervienen en el comportamiento del sistema. Inicialmente se obtuvo el modelo matemático para la obtención de la parte real de la Permitividad, con la cual, después de haber realizado las simulaciones, mediciones y comprobaciones pertinentes se desarrolló en cambio el modelo para la obtención de la Permitividad compleja, es decir calcular tanto el valor real como el imaginario de esta magnitud.

Finalmente para poder validar estos modelos obtenidos, se realizaron varios script en Matlab, primeramente para simular el comportamiento del sistema frente a una muestra de dieléctrico y posteriormente para procesar los datos obtenidos en las mediciones del sistema ya implementado.

Los resultados de las simulaciones fueron comparados con los obtenidos en las mediciones y estos a su vez con los valores de materiales conocidos y expuestos en la literatura.

Rende (Cosenza),

*Paúl David Moreno Avilés*

Noviembre 2015

---

# Contents

|          |  |    |
|----------|--|----|
| <b>1</b> | <b>State of the Art</b> .....  | 1  |
| 1.1      | Methods for Permittivity Measurement. ....   | 1  |
| 1.1.1    | Material Characterization in Free Space. ....  | 1  |
| 1.1.1.1  | Short Cut Reflection .....   | 2  |
| 1.1.1.2  | Nicolson-Ross-Weir (NRW) Algorithm. ....   | 3  |
| 1.1.2    | Material Characterization using contact methods. ....  | 6  |
| 1.1.2.1  | Material Characterization using microwave frequencies with a micro-strip transmission line. .... | 6  |
| 1.1.2.2  | Material Characterization using a patch Antenna. ....  | 9  |
| 1.1.2.3  | Materials Characterization using a Resonant Cavity. ....   | 13 |
| 1.2      | Theoretical framework in which the research is based .....                                       | 19 |
| 1.2.1    | Radar Techniques .....   | 19 |
| 1.2.2    | Software Defined Radar (SDR) .....   | 20 |
| 1.2.2.1  | Signal Generation Through FMCW .....   | 22 |
| 1.2.2.2  | Signal Generation Through OFDM .....   | 27 |
| 1.2.3    | OFDM Multi-band .....  | 31 |
| 1.3      | Scientific Background Research .....   | 32 |
| 1.3.1    | NI USRP-2920 Card Applications .....   | 32 |
| 1.3.2    | Radar applied to Permittivity Measurement .....  | 34 |
| <b>2</b> | <b>Research Development</b> .....  | 39 |
| 2.1      | Support Theory .....   | 39 |
| 2.1.1    | Complex Permittivity. ....   | 39 |
| 2.1.2    | Propagation in the mediums .....   | 43 |
| 2.1.3    | Transmission and Reflection of a signal in Materials. ...  | 45 |
| 2.2      | Measurement Methodology. ....  | 48 |
| 2.3      | Mathematical Modelling .....   | 48 |
| 2.4      | Equipment and devices used .....   | 52 |

|          |  |           |
|----------|--|-----------|
| 2.4.1    | Anritsu 37269C Vector Network Analyzer, 40 MHz to 40 GHz ..... | 53        |
| 2.4.2    | Millimeter Products INC. 261K 595 Standard Gain Horns .....    | 53        |
| 2.4.3    | Anechoic Chamber of the $\mu WaveLab$ UNICAL .....             | 54        |
| 2.5      | Information Processing .....                                   | 56        |
| <b>3</b> | <b>Results and Discussion</b> .....                            | <b>59</b> |
| 3.1      | Data Collection .....  | 59        |
| 3.2      | Data validation and method evaluation. ....                    | 62        |
| 3.2.1    | Measuring Simulation System .....                              | 62        |
| 3.2.2    | Making several measurements .....                              | 63        |
| 3.2.3    | Comparison of results with known values .....                  | 64        |
| 3.3      | Comparison with similar techniques. ....                       | 65        |
| 3.4      | Advantages of using this technique. ....                       | 65        |
| <b>4</b> | <b>Conclusions</b> .....                                       | <b>67</b> |
| 4.1      | Conclusions. ....  | 67        |
| 4.2      | Suggestions .....  | 68        |
| 4.3      | Future Work .....  | 68        |
|          | <b>References</b> .....  | <b>69</b> |

---

## List of Figures

|      |  |    |
|------|--|----|
| 1.1  | Material Characterization in High Frequency . . . . .  | 2  |
| 1.2  | Basic Configuration for a dielectric measurement . . . . .   | 3  |
| 1.3  | NRW Algorithm Configuration . . . . .  | 5  |
| 1.4  | Transversal Section of a Micro-strip line. . . . .   | 6  |
| 1.5  | Micro-strip line with the Sample (taken from [14]) . . . . .   | 7  |
| 1.6  | Cell Parameters of the Micro-strip line . . . . .  | 7  |
| 1.7  | Micro-strip line Design (taken from [1]) . . . . .   | 8  |
| 1.8  | Micro-strip line implementation (taken from [1]) . . . . .   | 8  |
| 1.9  | Relationship between S21 Phase and Relative Dielectric<br>Constant (taken from [1]) . . . . .                                    | 9  |
| 1.10 | Several Dielectric Layers (taken from [14]) . . . . .  | 10 |
| 1.11 | Variation of Resonance frequency according to permittivity in<br>a patch antenna . . . . .                                       | 12 |
| 1.12 | Implementation of a patch antenna for Permittivity<br>measurement (taken from [1]) . . . . .                                     | 12 |
| 1.13 | Rectangular Cavity . . . . .   | 14 |
| 1.14 | Cylindrical Cavity . . . . .   | 15 |
| 1.15 | Cylindrical Dielectric Resonator. (taken from [1]) . . . . .   | 16 |
| 1.16 | Structure of a Cylindrical Resonant cavity. . . . .  | 16 |
| 1.17 | (a) Open resonator system and (b) equivalent circuit for the<br>impedance characterization of planar surfaces. (taken from [39]) | 18 |
| 1.18 | Basic Radar Scheme. . . . .  | 20 |
| 1.19 | Transmitted and Received Signal. . . . .   | 20 |
| 1.20 | Basic SDR scheme. . . . .  | 21 |
| 1.21 | Block diagram of Software Defined Measurement system. . . . .  | 21 |
| 1.22 | Linear Relationship (Frequency - Time) in a FMCW Signal. . . . .   | 22 |
| 1.23 | FMCW Signal. . . . .   | 23 |
| 1.24 | FMCW Frequency spectrum. . . . .   | 23 |
| 1.25 | Ranging with an FMCW system. . . . .   | 24 |
| 1.26 | Common modulation pattern for an FM-CW radar. . . . .  | 25 |
| 1.27 | Relationships with triangular modulation pattern. . . . .  | 27 |

XVIII List of Figures

|      |  |    |
|------|--|----|
| 1.28 | Diagram of an OFDM Signal Generation. (Taken from [20]) . . . .  | 28 |
| 1.29 | OFDM Signal Generation. . . . .  | 29 |
| 1.30 | OFDM Radar Block Diagram. . . . .  | 30 |
| 1.31 | OFDM Multi-band Generation. (Taken from [20]) . . . . .  | 31 |
| 1.32 | Spectrum of OFDM multi-band signal . . . . .   | 31 |
| 1.33 | Reflection of a wave in a medium change . . . . .  | 34 |
| 2.1  | Dielectric Permittivity spectrum over a wide range of frequencies. . . . .   | 42 |
| 2.2  | Propagation of an Electromagnetic Wave . . . . .   | 44 |
| 2.3  | Refracted Signal . . . . .   | 46 |
| 2.4  | System Scheme for Complex Permittivity Measurement . . . . .   | 48 |
| 2.5  | Normalized Radargram of two measurements . . . . .   | 51 |
| 2.6  | Anritsu 37269C Vector Network Analyzer . . . . .   | 53 |
| 2.7  | 261K 595 Standard Gain Horn. . . . .   | 54 |
| 2.8  | <i>μWaveLab</i> Logo . . . . .   | 55 |
| 2.9  | Inside the Anechoic Chamber . . . . .  | 55 |
| 2.10 | Monitoring System . . . . .  | 56 |
| 2.11 | Received Signal in a TXT File . . . . .  | 56 |
| 3.1  | Detailed Scheme of the measurement system . . . . .  | 60 |
| 3.2  | Calibration Measurement (Directly to the PEC) . . . . .  | 60 |
| 3.3  | Dielectric Measurement . . . . .   | 60 |
| 3.4  | Text Processing from the .txt file received in the VNA to the .mat file, used in the Algorithm in Matlab . . . . . | 61 |
| 3.5  | File .mat of a received signal just with necessary information . .   | 61 |
| 3.6  | Brief diagram of the algorithm in matlab . . . . .   | 62 |
| 3.7  | Simulation permittivity measurement system . . . . .   | 63 |
| 3.8  | Radargram obtained from Measurements . . . . .   | 64 |
| 3.9  | Relative Permittivity and Loss Tangent of wood sample. . . . .   | 64 |



---

## List of Tables

|     |   |    |
|-----|---|----|
| 1.1 | Relationship between bandwidth and other parameters. . . . .  | 25 |
| 1.2 | Software and hardware specification USRP Vs. USRP NI 2920 .   | 32 |
| 3.1 | Comparison between known values and measured values of<br>real Permittivity and Loss tangent of wood. . . . . | 65 |



## State of the Art

As an introduction of this work, a general review of characterization methods of dielectrics is explained, followed by a theoretical introduction of the principles and the different variations of these.

### 1.1 Methods for Permittivity Measurement.

There are diverse techniques that can be used to characterize the dielectric of the material of interest, focusing on the study of the radar echoes. This technique is important to obtain the complex relative dielectric permittivity which defines the reflective properties of each material.

Several methods of material's characterization have been well developed by previous works, but in separate ways. The main methods are: microstrip line, patch antenna and resonant cavity [1], [2], [3]. There are also non-contact characterization methods that use antennas, which provides information about the radiated material [1]. This is shown in figure 1.1.

#### 1.1.1 Material Characterization in Free Space.

This type of characterization is used when the dimensions of the sample are comparable with the wavelength. Moreover, the far-field conditions and a suitable measurement environment have to be reached.

##### **Far Field Condition:**

To guarantee that the incident wave against the sample is considered as a plane wave, the distance  $d$  between the transmission antenna and the sample has to satisfy the relationship:

$$d > \frac{2D^2}{\lambda} \quad (1.1)$$

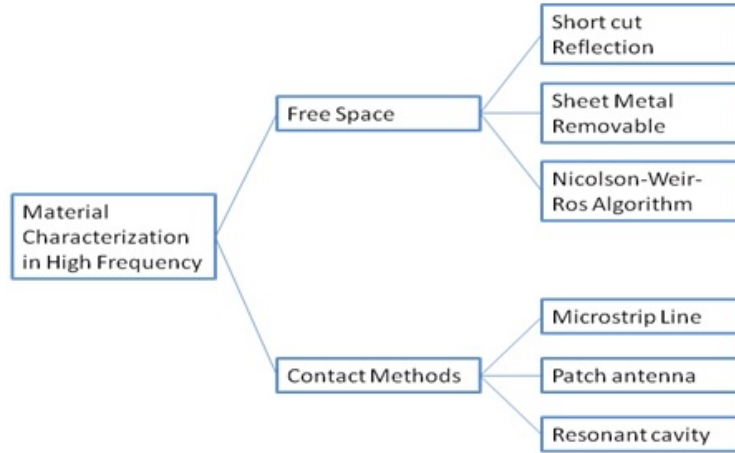


Fig. 1.1. Material Characterization in High Frequency

In the relationship shown above,  $\lambda$  is the wavelength of the operation frequency and  $D$  is the max value of the antenna aperture. If the condition of far field has been accomplished, then is possible to consider the system as a transmission line.

#### Sample's Size Condition:

When the sample is twice the dimensions of the wavelength of the operation frequency, it is assumed the Material Measurements in free space. This assumption is related to the fact that the size of the sample is smaller than the wavelength at the operation frequency. Then, the behaviour of the sample will be considered as a punctual particle, not as a complete one.

#### Measurement Environment Condition:

It is advisable to do the measurements in Electromagnetic Clean Environment; with anechoic chamber characteristics. In order to avoid undesired reflections, it is also required that, at lower frequencies, the sample does not have sudden ending's

##### 1.1.1.1 Short Cut Reflection

The figure 1.2 shows the configuration of an assemblage of a short-cut measurement system in free-space. The sample has a metal sheet in the back and it accomplishes the far-field condition.

It is possible analyse this configuration as a transmission line and relate it with the  $S_{11}$  parameter, in this way:

$$S_{11} = \frac{jZ \tan(\beta d) - 1}{jZ \tan(\beta d) + 1} \quad (1.2)$$

Where,  $Z$  is the wave impedance of the material under test normalized to the free space wave impedance, and  $\beta$  is the phase coefficient in the material under test. For no magnetic materials, the wave impedance is:

$$x = \frac{1}{\sqrt{\epsilon_r}} \tag{1.3}$$

And the phase constant is:

$$\beta = \frac{2\pi}{\lambda} \sqrt{\epsilon_r} \tag{1.4}$$

Where,  $\lambda$  is the wavelength in free-space, and  $d$  is the thickness of the sample.

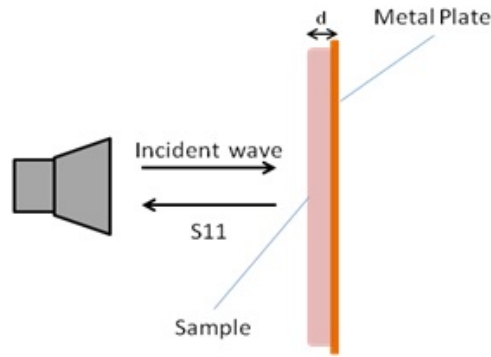


**Fig. 1.2.** Basic Configuration for a dielectric measurement

Figure 1.2 shows the use of a directive antenna that irradiates toward the sample with the metal sheet backrest. The reflection parameter  $S_{11}$  is measured with a vector network analyser; the previous relationships make the relative electric permittivity possible to calculate.

To implement this technique, it is necessary to use some electromagnetic simulation tools, such as HFSS from Ansoft, and Matlab for the processing data through a script. The mathematical models are found [1] and the dielectric constant of the sample is calculated by using numerical methods.

**1.1.1.2 Nicolson-Ross-Weir (NRW) Algorithm.**

Nicolson, Ross (1970) and Weir (1974) [9] proposed a way to obtain the dielectric constant of a material. The proposal consists in the measurement of the  $S_{11}$  and  $S_{21}$  parameters. Ghodgaonkar [10] implemented it to characterize materials in [11]. The equations obtained are:

$$S_{11} = \frac{\Gamma(1 - T^2)}{1 - \Gamma^2 T^2} \quad (1.5)$$

And

$$S_{21} = \frac{T(1 - \Gamma^2)}{1 - \Gamma^2 T^2} \quad (1.6)$$

Where  $\Gamma$  is the reflection coefficient in the boundary between the sample and the air:

$$\Gamma = \frac{z - 1}{z + 1} \quad (1.7)$$

And  $T$  is the transmission coefficient:

$$T = e^{-\gamma d} \quad (1.8)$$

Where  $\gamma$  is the propagation constant of the sample.  $\gamma$  and  $z$  are related to permittivity and permeability through the equations:

$$\gamma = \gamma_0 \sqrt{\varepsilon_r \mu_r} \quad (1.9)$$

$$z = \sqrt{\frac{\mu_r}{\varepsilon_r}} \quad (1.10)$$

With:

$$\gamma_0 = \frac{j2\pi}{\lambda_0} \quad (1.11)$$

Where  $\gamma_0$  is the propagation constant in free space, and  $\lambda_0$  is the wavelength in free space.

Considering the previous mathematical equations and manipulating them in order to find the variables of interest, we can calculate the relative dielectric constant. Then:

$$\Gamma = K \pm \sqrt{K^2 - 1} \quad (1.12)$$

$$T = \frac{S_{11} + S_{21} - \Gamma}{1 - (S_{11} + S_{21})\Gamma} \quad (1.13)$$

With

$$K = \frac{S_{11}^2 - S_{21}^2 + 1}{2S_{11}} \quad (1.14)$$

The positive or negative sign is chosen as a result of the condition that  $|\Gamma| < 1$ . From equation 1.8 the complex propagation constant  $\gamma$  is obtained in this way:

$$\gamma = \frac{\ln\left(\frac{1}{\Gamma}\right)}{d} \tag{1.15}$$

From equations 1.6 to 1.9 we get:

$$\sqrt{\frac{\mu_r}{\varepsilon_r}} = \left(\frac{1 + \Gamma}{1 - \Gamma}\right) \tag{1.16}$$

And from equations 1.9 to 1.16 we have:

$$\varepsilon_r = \frac{\gamma}{\gamma_0} \left(\frac{1 - \Gamma}{1 + \Gamma}\right) \tag{1.17}$$

$$\mu_r = \frac{\gamma}{\gamma_0} \left(\frac{1 + \Gamma}{1 - \Gamma}\right) \tag{1.18}$$

In this particular case, it is important to know about the dielectric constant, in order to calculate the reflectivity [12] of a sample under test. The reflectivity is given by the next relationship:

$$R = \frac{(\sqrt{\varepsilon_r} - 1)^2}{(\sqrt{\varepsilon_r} + 1)^2} = |\Gamma|^2 \tag{1.19}$$

Where equation 1.19 is the relationship between the energy that the radar antenna radiates and the energy that comes back as a reflected wave to the starting point.

The Figure 1.3 illustrates the configuration of this method of materials characterization, using the NRW algorithm.

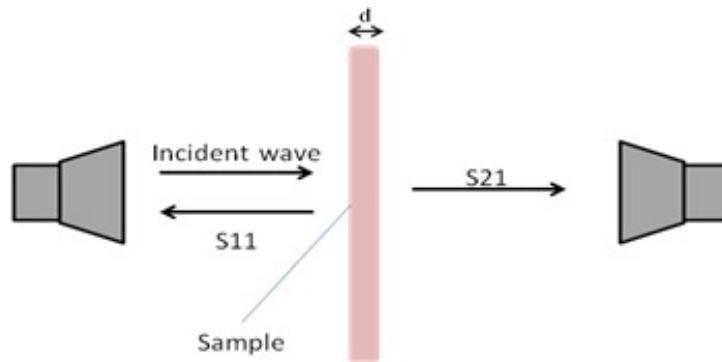


**Fig. 1.3.** NRW Algorithm Configuration

### 1.1.2 Material Characterization using contact methods.

This section presents the configuration of material characterization that requires contact. It is also necessary to use a sample of a substance to characterize the electric properties.

#### 1.1.2.1 Material Characterization using microwave frequencies with a micro-strip transmission line.

With the implementation of a transmission line, it is possible to characterize materials through the measurement of S11 and S21 parameters. Further analysis are described in [13] and [14].

The first step in this method is the determination of the parameters of dispersion of the micro-strip line. As it is shown in Figure 1.4, the transversal section of the line consists in a structure of shielded micro-strip, which is composed of a container for the sample, a thin sample and its respective support. Figure 1.5 shows the aspect of the transmission line and the sample under test.

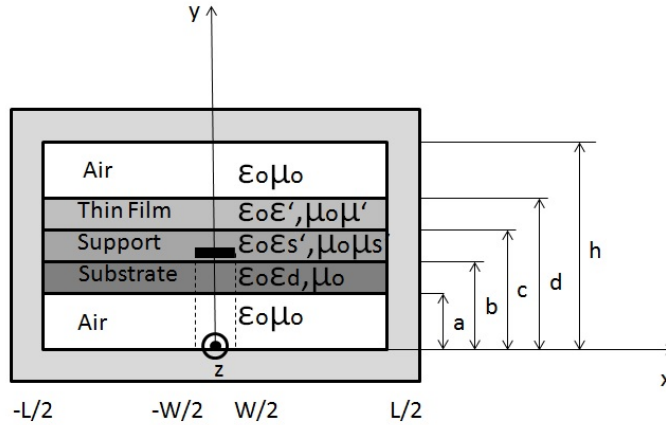


Fig. 1.4. Transversal Section of a Micro-strip line.

The second step of this method consists in calculating the parameter's setup of the conditions of electromagnetic continuity, as it is shown in Figure 1.6. The use of the orthogonality in the modes makes it possible to find the engage coefficients  $\rho_n, t_n, R_n, T_n$  among the modes, in order to reach the conditions of continuity.

The cell parameters of the micro-strip line are given by the next equations:

$$S_{11} = S_{22} = \rho_1 e^{-2j\gamma_0 l_0} \quad (1.20)$$



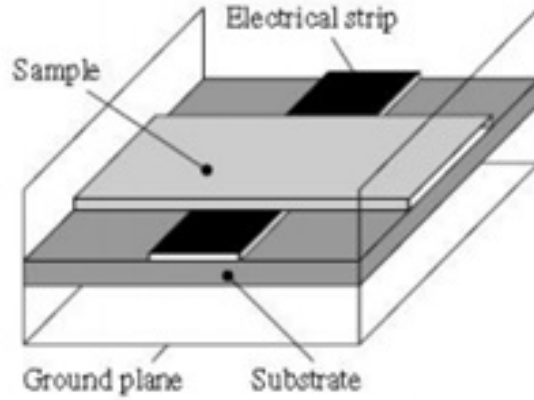


Fig. 1.5. Micro-strip line with the Sample (taken from [14])

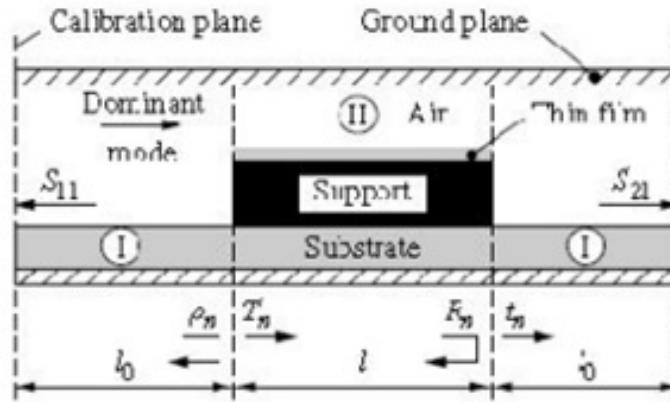


Fig. 1.6. Cell Parameters of the Micro-strip line

$$S_{21} = S_{12} = t_1 e^{-2j\gamma_0 l_0} \tag{1.21}$$

Where  $t_1$  and  $\rho_1$  represent the transmission and reflection coefficients of the fundamental mode across the cell discontinuities.

To make this theory possible, several tests, as the ones that are explained in [1], have been done. In this case, a transmission line was implemented in the simulator of high-frequency HFSS from Ansoft. Then a sample of material was placed in this line. The dielectric constant of the material was defined as a variable whose value can change. Finally, the parameters  $S_{11}$  and  $S_{21}$  as the results required by the analysis are obtained.

Figure 1.7 and Figure 1.8 expose the implementation of the transmission line in the simulator and the realization, respectively, with the sample on it.

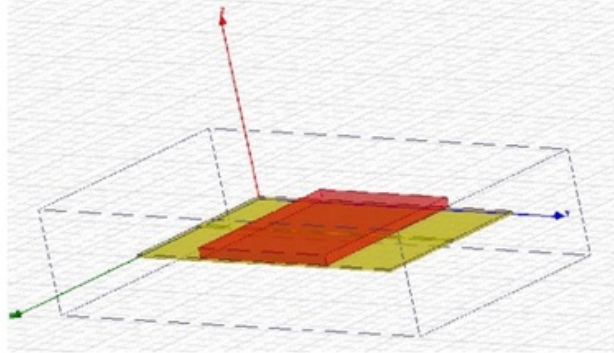


**Fig. 1.7.** Micro-strip line Design (taken from [1])

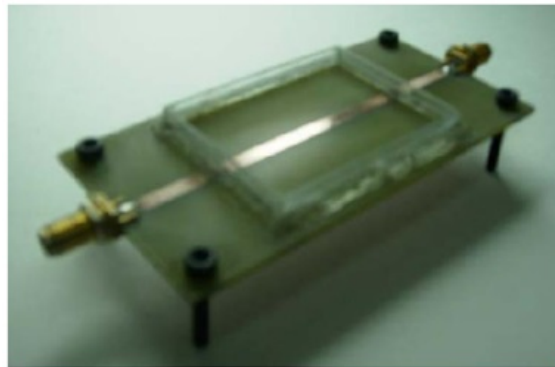


**Fig. 1.8.** Micro-strip line implementation (taken from [1])

In the results of the simulation, the maximum interest information is the phase of the parameter  $S_{21}$ , because this varies in a proportional way with the material dielectric constant, as it is presented in Figure 1.9. In this graphic, it is possible to obtain a tabulation of dielectric constant related to the  $S_{21}$  phase, it makes it easier to obtain the dielectric constant of a material.

In the Figure 1.9 the proportionality between the  $S_{21}$  phase and the relative dielectric constant is shown. It is important to emphasize that this technique permits to characterize dielectric fluids with relative dielectric constants that are lower than 80. Beyond this value, duality problems in the measurement are presented.

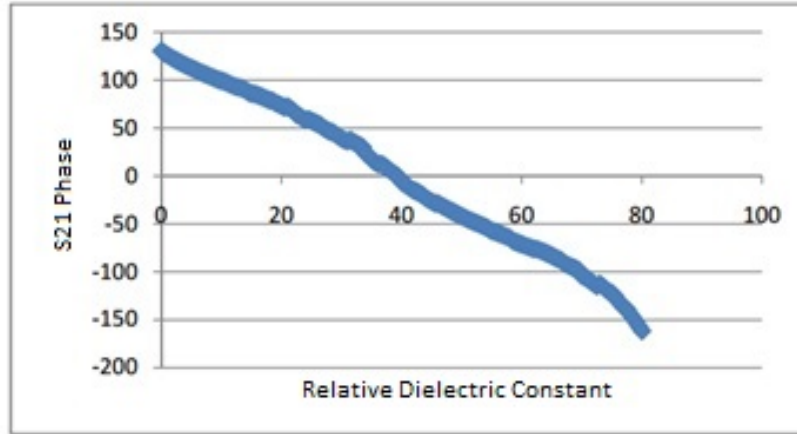


**Fig. 1.9.** Relationship between S21 Phase and Relative Dielectric Constant (taken from [1])

Starting from the measurements taken in tests made in [1] it is possible to conclude that the results of this method are coherent according to the literature consulted in the research related to the relative dielectric constant of materials.

This method is quite easy to implement too, because of its low-cost and fast measuring. Moreover, big resources of hardware are not required when the method is simulating. As a result of everything that has been mentioned, this method becomes a fast and effective way to solve problems when it is necessary to make materials characterization using microwaves.

### 1.1.2.2 Material Characterization using a patch Antenna.

This method uses a patch antenna just as it is designed according to [15]. A dielectric sample is placed in the patch antenna, which changes the resonance frequency of the antenna in comparison to how it was empty, Considering this principle; it is possible to determine the relative dielectric constant and the loss tangent of the dielectric measured. In the case of a  $n$  embed antenna, in several dielectric layers, we can have a transversal configuration, as it is shown in Figure 1.10

The antenna resonance frequency ( $f_r$ ) changes according to the value of the effective dielectric constant ( $\epsilon_{eff}$ ) and the antenna dimensions:

$$f_r = \frac{c}{2(l + 2\Delta L)\sqrt{\epsilon_{eff}}} \quad (1.22)$$

To analyse this phenomenon, it is necessary to take into account the effective permittivity  $\epsilon_{eff}$ . However, a review of the concept of quasi static

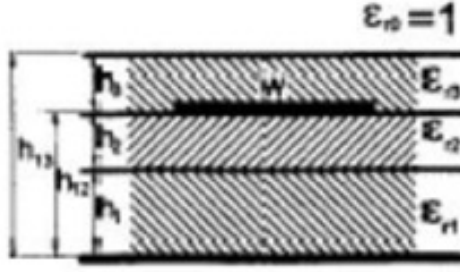


**Fig. 1.10.** Several Dielectric Layers (taken from [14])

effective permittivity  $\varepsilon_e$  is required to make before. That depends on the relationship between geometry and permittivity of each layer superimposed. The expression for quasi static effective permittivity is:

$$\varepsilon_e = \varepsilon_{r1}\varepsilon_{r2} \frac{(q_1 + q_2)^2}{\varepsilon_{r1}q_2 + \varepsilon_{r2}q_1} + \varepsilon_{r3} \frac{(1 - q_1 - q_2)^2}{\varepsilon_{r3}(1 - q_1 - q_2 - q_3) + q_3} \quad (1.23)$$

Where:

$$q_1 = \frac{S_1}{S_c} = \frac{h_1}{2h_{12}} \left\{ 1 + \frac{\pi}{4} - \frac{h_{12}}{\omega_e} * \ln \left[ \frac{\omega_e}{h_1} \sin \left( \frac{\pi h_1}{2h_{12}} \right) + \cos \left( \frac{\pi h_1}{2h_{12}} \right) \right] \right\} \quad (1.24)$$

$$q_2 = \frac{S_2}{S_c} = 1 - q_1 - \frac{h_{12}}{\omega_e} * \ln \left[ \frac{\pi \omega_e}{h_{12}} - 1 \right] \quad (1.25)$$

$$q_3 = 1 - q_1 - q_2 - \frac{h_{12} - v_e}{2\omega_e} \ln \left[ \frac{2\omega_e}{2h_{13} - h_{12} + v_e} \cos \left( \frac{\pi v_e}{2h_{12}} \right) + \sin \left( \frac{\pi v_e}{2h_{12}} \right) \right] \quad (1.26)$$

$$\omega_e = W + \frac{2h_{12}}{\pi} \ln \left[ 17.08 \left( \frac{W}{2h_{12}} + 0.92 \right) \right] \quad (1.27)$$

$$v_e = \frac{2h_{12}}{\pi} \tan^{-1} \left[ \frac{2\pi}{\pi\omega_e - 4h_{12}} (h_{13} - h_{12}) \right] \quad (1.28)$$

The effective relative permittivity is obtained in base of the quasi-static permittivity before calculated:

$$\varepsilon'_r = \frac{2\varepsilon_e - 1 - A}{1 + A} \quad (1.29)$$

Where:

$$A = \left(1 + \frac{12h_{12}}{W}\right)^{-\frac{1}{2}} \quad (1.30)$$

On the other hand, this technique permits to obtain the loss tangent of a material, through the measurement of the antenna quality factor [15]. Then:

$$\frac{1}{Q_T} = \frac{1}{Q_{rad}} + \frac{1}{Q_c} + \frac{1}{Q_d} + \frac{1}{Q_{SW}} \quad (1.31)$$

Where

$\frac{1}{Q_T}$  is the total quality factor,

$\frac{1}{Q_{rad}}$  is the factor quality caused by the radiation losses,

$\frac{1}{Q_c}$  is the quality factor caused by the conduction losses,

$\frac{1}{Q_d}$  is the quality factor caused by the dielectric losses (when the substrates are very thin, it is allowed to ignore this value)

When the substrates are very thin is allowed to ignore the quality factor caused by surface waves  $\frac{1}{Q_{SW}}$ . Every factor earlier mentioned is expressed in this way:

$$Q_c = h\sqrt{\pi f \mu \sigma} \quad (1.32)$$

$$Q_d = \frac{1}{\tan(\delta)} \quad (1.33)$$

$$Q_{rad} = \frac{2\omega\varepsilon_r}{h\frac{L}{t}}K \Rightarrow K = \frac{L}{4} \text{ and } G_{\frac{t}{L}} = \frac{G_{rad}}{W} \quad (1.34)$$

$Q_d$  and  $Q_c$  are the quality factors when there is not a super substrate [16], and  $Q_{tS}$  and  $Q_{radS}$  are the quality factors with a super substrate, then:

$$\frac{1}{Q_{t0}} = \frac{1}{Q_{rad0}} + \frac{1}{Q_c} + \frac{1}{Q_d} \quad (1.35)$$

$$\frac{1}{Q_{tS}} = \frac{1}{Q_{radS}} + \frac{1}{Q_c} + \frac{1}{Q_d} \quad (1.36)$$

When a super substrate is added, there is one difference in the losses in comparison to how it is when it does not have a substrate. In this mode, the loss tangent of the superimposed dielectric sample is:

$$\tan(\delta_s) = \Delta \left( \frac{1}{Q_t} + \frac{1}{Q_{t0}} + \frac{1}{Q_{tS}} \right) \quad (1.37)$$

Considering this theoretical basis, several tests have been implemented in [1], with the electromagnetic simulator of high-frequency HFSS from Ansoft. The simulation is similar to the one that was implemented in the micro-strip line method. The antenna must be designed in the simulator, then the

dielectric sample is placed on the antenna. Its permittivity changes in the simulator so do the value of the antenna resonance frequency. This change permits to obtain the relative dielectric constant and the loss tangent of the material.

Then, with the data obtained, a Matlab script is necessary to make all calculations and operations required for the characterization of the dielectric properties of interest. Knowing the resonance frequency values, the antenna dimensions and the type of dielectric measured.

This procedure is summarized and diagrammed in the Figure 1.11.

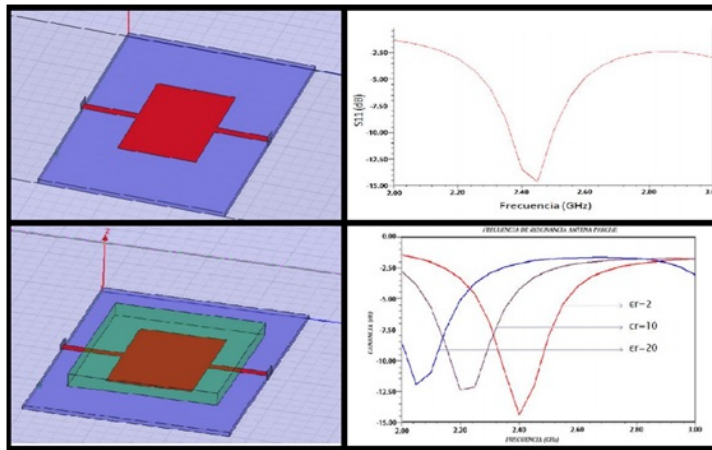


**Fig. 1.11.** Variation of Resonance frequency according to permittivity in a patch antenna

And the implementation is shown in the Figure 1.12.

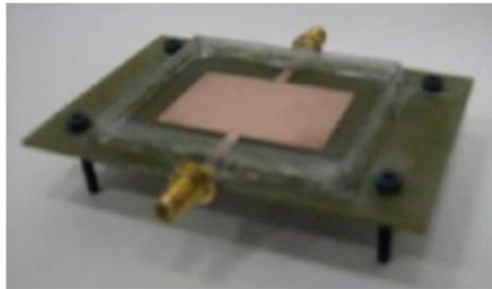


**Fig. 1.12.** Implementation of a patch antenna for Permittivity measurement (taken from [1])

### 1.1.2.3 Materials Characterization using a Resonant Cavity.

A Resonant Cavity is a special type of resonator, consisting of a closed (or largely closed) metal structure that confines electromagnetic fields in the microwave region of the spectrum. The structure is either hollow or filled with dielectric material.

A microwave cavity acts similarly to a resonant circuit with extremely low loss at its frequency of operation, resulting in quality factors up to the order of  $10^6$ , compared to  $10^2$  for circuits made with separate inductors and capacitors at the same frequency. They are used in oscillators and transmitters to create microwave signals, and as filters to separate a signal at a given frequency from other signals, in equipment such as radar equipment, microwave relay stations, satellite communications, and microwave ovens.

In addition to their use in electrical networks, resonant cavities can manipulate charged particles passing through them by application of acceleration voltage and are thus used in particle accelerators.

Most resonant cavities are made from closed (or short-circuited) sections of waveguide or high-permittivity dielectric material. Electric and magnetic energy is stored in the cavity and the only losses are due to finite conductivity of cavity walls and dielectric losses of material filling the cavity. Every cavity has numerous resonant frequencies that correspond to electromagnetic field modes satisfying necessary boundary conditions on the walls of the cavity. Because of these boundary conditions that must be satisfied at resonance (tangential electric fields must be zero at cavity walls). It follows that cavity length must be an integer multiple of half-wavelength at resonance [13]. Hence, a resonant cavity can be thought of as a wave-guide equivalent of short circuited half-wavelength transmission line resonator [13]. Q factor of a resonant cavity can be calculated using cavity perturbation theory and expressions for stored electric and magnetic energy.

The electromagnetic fields in the cavity are excited via external coupling. An external power source is usually coupled to the cavity by a small aperture, a small wire probe or a loop [40]. External coupling structure has an effect on cavity performance and needs to be considered in the overall analysis [41].

The quality factor  $Q$  of a cavity can be decomposed into three parts, representing different power loss mechanisms:

$Q_c$  Resulting from the power loss in the walls which have finite conductivity;

$Q_d$  Resulting from the power loss in the lossy dielectric material filling the cavity;

$Q_{ext}$  resulting from power loss through unclosed surfaces of the cavity geometry; this term can be normally ignored in a Resonant Cavity Analysis and the total Q factor of the cavity can be found as:

$$Q = \left( \frac{1}{Q_c} + \frac{1}{Q_d} \right)^{-1} \quad (1.38)$$

The Cavity geometry more developed due to the simplicity of the equations are the Rectangular Cavity and the Circular Cavity.

In a Rectangular Cavity, Resonance frequencies for any  $TE_{mnl}$  or  $TM_{mnl}$  resonant mode can be found by imposing boundary conditions on electromagnetic field expressions. This frequency is given by [13]

$$f_{mnl} = \frac{c}{2\pi\sqrt{\mu_r\epsilon_r}}k_{mnl} \quad (1.39)$$

Developing

$$f_{mnl} = \frac{c}{2\sqrt{\mu_r\epsilon_r}}\sqrt{\left(\frac{m}{a}\right)^2 + \left(\frac{n}{b}\right)^2 + \left(\frac{l}{d}\right)^2} \quad (1.40)$$

Where  $k_{mnl}$  is the wave-number, with  $m, n, l$  being the mode numbers and  $a, b, d$  being the corresponding dimensions as in Figure 1.13;  $c$  is the speed of light in vacuum; and  $\mu_r$  and  $\epsilon_r$  are relative permeability and permittivity of the cavity filling respectively.

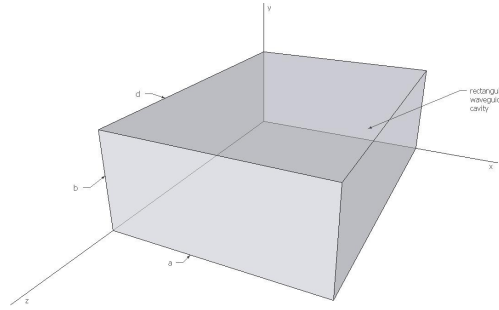


**Fig. 1.13.** Rectangular Cavity

In a cylindrical cavity of length  $L$  and radius  $R$  (Figure 1.14) the field solutions follow from the solutions of a cylindrical wave-guide with additional electric boundary conditions at the position of the enclosing plates. The resonance frequencies are different for TE and TM modes [42].

In TM modes:

$$f_{nmp} = \frac{c}{2\sqrt{\mu_r\epsilon_r}}\sqrt{\left(\frac{X_{mn}}{R}\right)^2 + \left(\frac{p\pi}{L}\right)^2} \quad (1.41)$$

In TE modes

$$f_{nmp} = \frac{c}{2\sqrt{\mu_r\epsilon_r}}\sqrt{\left(\frac{X'_{mn}}{R}\right)^2 + \left(\frac{p\pi}{L}\right)^2} \quad (1.42)$$



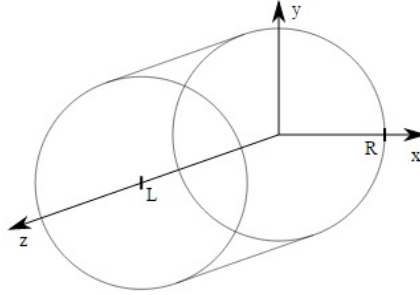


**Fig. 1.14.** Cylindrical Cavity

Here,  $X_{mn}$  denotes the  $n$ -th zero of the  $m$ -th Bessel function, and  $X'_{mn}$  denotes the  $n$ -th zero of the derivative of the  $m$ -th Bessel function.

Then, with this kind of cavities it is possible to characterize a dielectric material, through the measurements of the quality factor and the variations of its value according to the dielectric that has been used.

This type of methods, unlike those in which there is no transmission and reflection (Section 1.1.1) is not capable of performing measurements with a sweep in wide frequency. The other ones are only adaptable to a desired frequency, based on the theory of perturbation [35]. However, the measurement of dielectric properties, by resonance methods, presents greater accuracy, especially in low dielectric materials or magnetic loss. Therefore, resonance methods are most often used [9] [14].

The fundamental concept of resonance method is based on the presence of a small sample of a dielectric or magnetic material in a resonant cavity. This will cause a change in the resonant frequency and a decrease in the quality factor of the cavity. A small sample refers to the volume of the sample is much smaller compared to the volume of the cavity. This means that changing the electric or magnetic field is small [37].

The permittivity of the material can be calculated from the changes of the resonance frequency and quality factor of the resonant cavity. Cylindrical and rectangular cavities are commonly adapted for this purpose, because the equations of the electric and magnetic fields are easier to lead to simple geometries. The sample should always be placed where the electric or magnetic field (depending on the case) present the higher current [37].

The system consists in a resonant cavity, where the sample measured, a microwave generator and a receiver comprising, a directional coupler and a microwave detector are placed. The resonant cavity is connected to the input port of a directional coupler, while the microwave detector is connected to the coupled port of directional coupler, to detect the changes of the resonance frequency due to the sample placed in the cavity resonant.

Actually, in several pieces of works, the cavity for dielectric characterization that is used the most is the cylindrical resonator, which permits to

measure the permittivity of liquid substances. The construction of these devices is based on a circular waveguide, with a shortcut in both terminals, as it is shown in Figure 1.15.



**Fig. 1.15.** Cylindrical Dielectric Resonator. (taken from [1])

This type of cavity has a resonant mode  $TE_{111}$ . The resonance frequency of this type of wave guide is based on the  $TE_{nml}$  and  $TM_{nml}$  modes, and the expression of the quality factor for the  $TE_{nml}$  mode. The figure 1.16 shows the typical structure of a cylindrical resonant cavity.

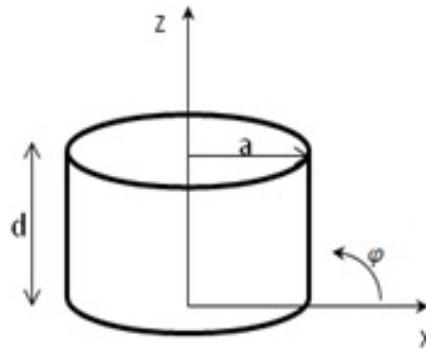


**Fig. 1.16.** Structure of a Cylindrical Resonant cavity.

The transversal electrical fields ( $E_\rho$  and  $E_\varphi$ ) of the wave guide modes are described with the next relationship:

$$E_{t(\rho,\varphi,z)} = \bar{e}_{t(\rho,\varphi)} [A^+ e^{-j\beta_{nm}} + A^- e^{j\beta_{nm}}] \quad (1.43)$$

Where  $\bar{e}_{t(\rho,\varphi)}$  represents variations in transversal mode. The amplitudes  $A$  represent the magnitudes of the transmitted and reflected wave. The factor  $\beta$  represents the propagation constant in the  $TE_{nm}$  mode. This factor is expressed with the next equation:

$$\beta_{nm} = \sqrt{k^2 - \left(\frac{\rho'_{nm}}{a}\right)^2} \quad (1.44)$$

In the  $TM_{nm}$  mode, the propagation constant is:

$$\beta_{nm} = \sqrt{k^2 - \left(\frac{\rho_{nm}}{a}\right)^2} \quad (1.45)$$

Where  $k$  is the wave number and is represented in this way:  $k = \omega\sqrt{\mu\epsilon}$ .

From [17] it is known that the resonance frequency for the  $TE_{nm}$  mode of a cylindrical wave guide is:

$$f_{nml} = \frac{c}{2\pi\sqrt{\mu_r\epsilon_r}} \sqrt{\left(\frac{\rho'_{nm}}{a}\right)^2 + \left(\frac{l\pi}{d}\right)^2} \quad (1.46)$$

And for the  $TM_{nml}$  mode, the resonance frequency is:

$$f_{nml} = \frac{c}{2\pi\sqrt{\mu_r\epsilon_r}} \sqrt{\left(\frac{\rho_{nm}}{a}\right)^2 + \left(\frac{l\pi}{d}\right)^2} \quad (1.47)$$

The key of this material characterization technique consists in making the measurements of the cavity resonance in order to get the relative dielectric constant of the material. For this situation, the  $TE_{111}$  mode is the dominant mode. The equations that define the fields for this modes are:[17]

$$H_z = H_0 J_n \left(\frac{P'_{nm}\rho}{a}\right) \cos(n\varphi) \sin \frac{l\pi z}{d} \quad (1.48)$$

$$H_\rho = \frac{\beta_0 H_0}{P'_{nm}} J_n \left(\frac{P'_{nm}\rho}{a}\right) \cos(n\varphi) \cos \frac{l\pi z}{d} \quad (1.49)$$

$$H_\varphi = \frac{-\beta a^2 n H_0}{(P'_{nm})^2 \rho} J_n \left(\frac{P'_{nm}\rho}{a}\right) \sin(n\varphi) \cos \frac{l\pi z}{d} \quad (1.50)$$

$$E_\rho = \frac{jk\eta a^2 n H_0}{(P'_{nm})^2 \rho} J_n \left(\frac{P'_{nm}\rho}{a}\right) \sin(n\varphi) \sin \frac{l\pi z}{d} \quad (1.51)$$

$$E_\varphi = \frac{jk\eta a H_0}{P'_{nm}} J_n \left(\frac{P'_{nm}\rho}{a}\right) \cos(n\varphi) \sin \frac{l\pi z}{d} \quad (1.52)$$

Where  $\eta = \sqrt{\frac{\mu}{\epsilon}}$  and  $H_0 = -2jA^+$  and in the  $TE_{111}$  mode  $\rho_{nm} = 1.841$ .

With this technique, it is possible to find the loss tangent of a liquid dielectric. This can be achieved through the quality factor, which can be calculated with this relationship:

$$\frac{1}{Q_T} = \frac{1}{Q_c} + \frac{1}{Q_d} \quad (1.53)$$

Where, as it was mentioned before,  $Q_c$  represents the quality factor caused by the conduction losses and  $Q_d$  represents the quality factor caused by the dielectric losses.

$$Q_c = \frac{W_0 W}{P_0} = \frac{(ka)^3 \eta a d \left(1 - \left(\frac{n}{P_{nm}}\right)^2\right)}{4(P'_{nm})^2 R_S \left\{ \frac{ad}{2} \left[1 + \left(\frac{\beta a n}{(P'_{nm})^2}\right)^2\right] + \left(\frac{\beta a n}{P'_{nm}}\right)^2 \left(1 - \frac{n^2}{(P'_{nm})^2}\right)\right\}} \quad (1.54)$$

and

$$Q_d = \frac{1}{\tan \delta} = \frac{f_0}{BW} \quad (1.55)$$

Finally, other kind of resonators called Open Resonator can be used for Dielectric Characterization [38], [39].

The open resonator system adopted for the equivalent impedance characterization is illustrated in Figure 1.17 (a). It consists of a spherical mirror of radius  $R_0$ , which is used to produce a Gaussian beam impinging on the grounded test surface at a distance  $l$ . A feeding rectangular wave-guide of standard height  $b$  is adopted for the cavity excitation, and a transition is properly designed to optimize the coupling with the cavity.

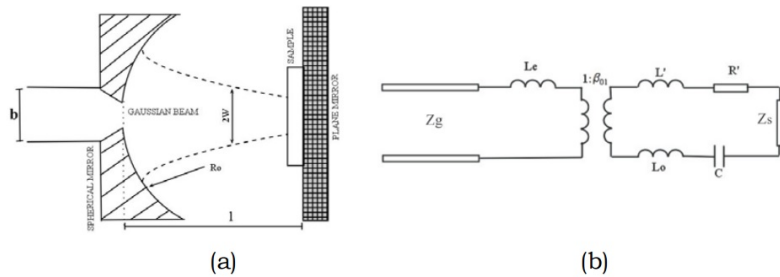


**Fig. 1.17.** (a) Open resonator system and (b) equivalent circuit for the impedance characterization of planar surfaces. (taken from [39])

The approach proposed in [43] is mentioned, which is based on a complete eigenfunctions analysis leading to the equivalent circuit of Figure 1.17 (b). The relative circuit parameters, accurately defined in [43], properly model the cavity losses, thus leading to an accurate characterization of the open resonator behaviour in the presence of the unknown test surface, whose equivalent impedance  $Z_s$  can be easily derived from return loss measurements performed at the wave-guide input, under empty and loaded cavity conditions. As a matter of fact, the insertion of the test surface sample produces a shift in the resonant frequency of the cavity, from which the imaginary part of impedance  $Z_s$  can be retrieved. At the same time, an amplitude reduction of the reflection coefficient is obtained in the presence of the test sample, which in turns is related to the real part of impedance  $Z_s$ .

For complex permittivity retrieval of thin dielectric substrates, the insertion of a grounded dielectric substrate having complex permittivity  $\varepsilon = \varepsilon' j\varepsilon''$  leads to an equivalent impedance  $Z_s$ , easily expressed as:

$$Z_s = jZ_d \tan(k_d h - \phi_G) \quad (1.56)$$

Where  $Z_d$  and  $k_d$  give the characteristic impedance and the propagation constant of the dielectric slab  $h$ , while  $\phi_G$  is the phase shift caused by the impinging Gaussian beam [44]. Equation 1.56 can be easily splitted into its real and imaginary parts, which are related to the unknown terms  $\varepsilon'$  and  $\varepsilon''$ . From the return loss measurements, the information relative to the resonant frequency shift and the loaded quality factor are derived, which are used to retrieve the imaginary and the real parts of impedance  $Z_s$ , respectively. In the final stage, the complex permittivity is reconstructed from the above information [44].

## 1.2 Theoretical framework in which the research is based

This section provides a summary of the techniques used for the development of research on which this thesis is based, beginning from the Software Defined Radar Theory (SDR) explaining every Signal Generation Techniques, among them FMCW and OFDM and emphasizing in the OFDM multi-band generation.

### 1.2.1 Radar Techniques

Radar is a system that uses electromagnetic waves to measure range, altitude, direction and speed from statics or moving targets such as aircraft, ships, vehicles, space craft and terrain. The operation consists in transmit a radio pulse, that will be reflected in the target, then the signal typically will come back to the source. Starting from this echo is possible to get a lot of information about the target, Figure 1.18.

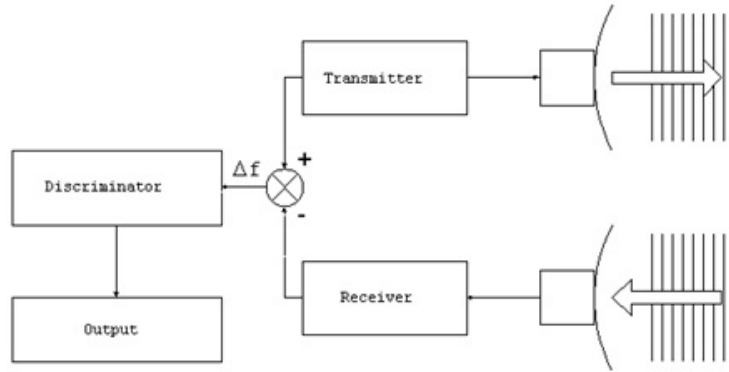


**Fig. 1.18.** Basic Radar Scheme.

The received signal arrives to the receiver antenna with a delay time respect to the original, caused by the trail distance from the source to the target and to the source again, that means two times the distance of the target from the source Figure 1.19.

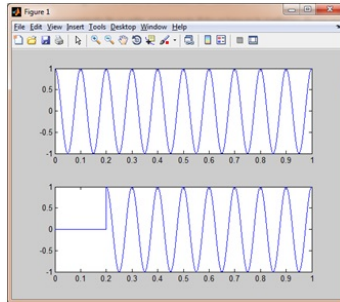


**Fig. 1.19.** Transmitted and Received Signal.

### 1.2.2 Software Defined Radar (SDR)

Radar systems technology reduces the usage of hardware (signal generators, mixers, modulators, filters), with implementations via software using embedded systems or FPGA. These systems are known as SDRadar (Software Defined Radar), reduce considerably the implementation costs with a lot of versatilities, capabilities and applications. As it is shown in Figure 1.20.

A classical radar measuring system is composed of dedicated hardware, depending of the application (Doppler, weather, Ground penetrating Radar, etc.). The new conception of Software Defined Radar provides a high degree of flexibility and adaptability to several signal processing techniques. In a

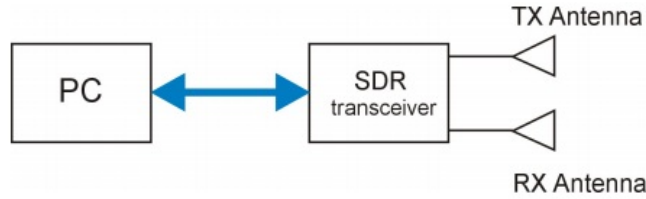


**Fig. 1.20.** Basic SDR scheme.

Software Defined Radar system most of the operations regarding to the signal processing are carried out via software; so it permits the creation of a multi-purpose radar, whose different algorithms for each application take place in the same device. In this work, a custom software defined transceiver is adopted as a low-cost measurement instrument, which is equipped with transmitting (TX) and receiving (RX) antennas. The necessary data processing algorithms are directly connected to a PC hosting. Therefore, by enabling the multi-purpose feature in terms of adaptability, it is possible to have a large variety of dielectric material’s characterization.

A block diagram of the proposed Software Defined system is shown in Figure 1.21.

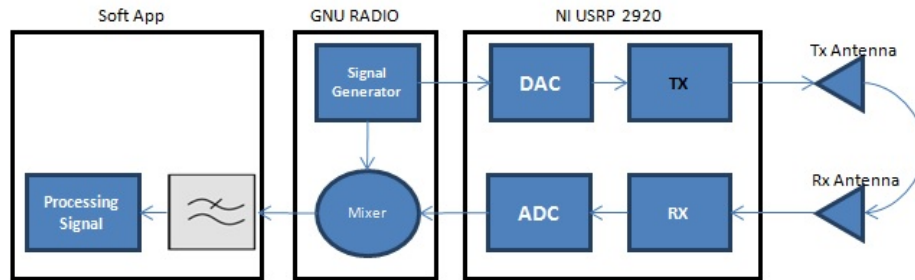


**Fig. 1.21.** Block diagram of Software Defined Measurement system.

The key of SDRadar is the Signal Generation, which is related to the type of signal that will be transmitted and then processed. There are various techniques that permit to generate one suitable application for SDRadar, The codification through modulation of binaries pulses train, modulation through Orthogonal signals (OFDM), or Frequency Modulation of Continuous Wave (FMCW) can be mentioned among the major ones.

Each of those techniques uses different mathematical models; for example, FMCW generates a sinusoidal signal whose frequency changes along the time. This means that frequency increases as long as time does it too. That type

of signal and its respective processing in frequency can be very useful to determine target distances, target movement and even velocity.

With these applications, it is possible to make some variations in the developing of radar software and create diverse systems, just changing the programming and processing data, such as calculation of relativity permittivity of a dielectric substrate.

### 1.2.2.1 Signal Generation Through FMCW

The Frequency Modulation of Continuous Wave is a Signal generation whose frequency changes linearly in function of time, as it is shown in Figure 1.22.

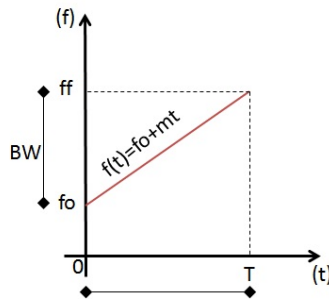


**Fig. 1.22.** Linear Relationship (Frequency - Time) in a FMCW Signal.

This is the linear mathematical relationship between the frequency vs time:

$$f(t) = f_0 + mt \quad (1.57)$$

Where:

$f(t)$  is the frequency in function of time  $t$ ,

$f_0$  represents the starting Frequency,

$m$  represents the variation pendant of the lineal relationship,

$T$  is the signal duration where the frequency reaches its maximum value  $f_f$  and

$BW$  is the bandwidth of the FMCW signal.

Then by applying this frequency in a sinusoidal signal, it is possible to create the FMCW signal:

$$g(t) = A \sin(2\pi f(t)t) \quad (1.58)$$

Being:

$g(t)$  the FMCW signal and

$A$  the amplitude of the signal.

In the Figure 1.23 it is possible to see the frequency increment according to time increment, in the time domain, in a linear way.



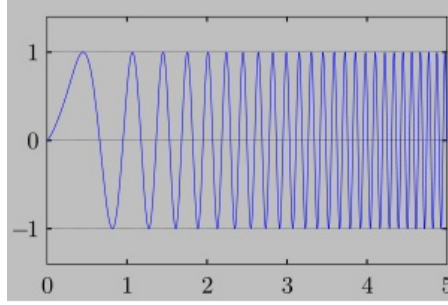


**Fig. 1.23.** FMCW Signal.

If the Fast Fourier Transform is applied to equation 1.58, we can see the bandwidth in which the signal works in the frequency domain, as it is shown in figure 1.24.

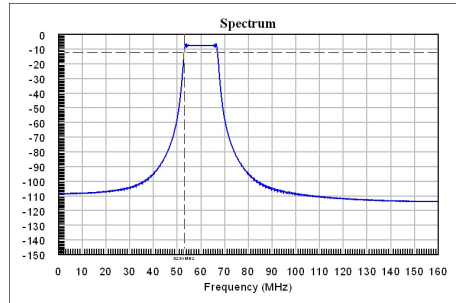


**Fig. 1.24.** FMCW Frequency spectrum.

When this signal is used in a radar system, the main advantage of FMCW signal is the fact that energy is not pulsed. As a result, this system is much easier to implement and operate and has no minimum or maximum range, even though the broadcast power level imposes a practical limit on range. Continuous-wave radar maximizes total power on a target because the transmitter is broadcasting continuously.

In this method, a signal is transmitted, which changes periodically in the frequency. When an echo signal is received, that change of frequency gets a delay  $\Delta t$  (by runtime shift) as in the pulse radar technique, then a comparison between the transmitted and received echo signal is done, Figure 1.25.

The distance  $R$  to the reflecting object can be determined by the following relationships:

$$R = \frac{c\Delta t}{2} = \frac{c\Delta f}{2(df/dt)} \tag{1.59}$$

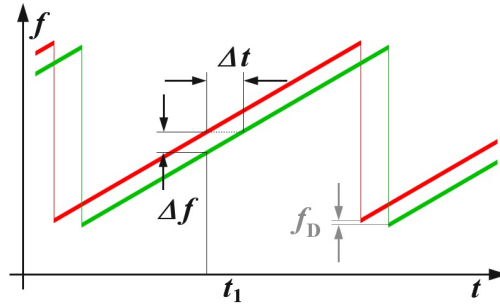


**Fig. 1.25.** Ranging with an FMCW system.

Where:

$c$  is the speed of light  $= 3 * 10^8 \frac{m}{s}$ ,

$\Delta t$  is the delay time [s],

$\Delta f$  is the measured frequency difference [Hz],

$R$  is the distance between antenna and the reflecting object [m] and

$df/dt$  is the frequency shift per unit of time

If the change in frequency is linear over a wide range, then the radar range can be determined by a simple frequency comparison. The frequency difference  $\Delta f$  is proportional to the distance  $R$ . Since only the absolute amount of the difference frequency can be measured (negative numbers for frequency does not exist), the results are at a linearly increasing frequency equal to a frequency decreasing (in a static scenario: without Doppler effects).

If the reflecting object has a radial speed related to the receiving antenna, then the echo signal gets a Doppler frequency  $f_D$  (caused by the speed). The radar measures not only the difference of frequency  $\Delta f$  to the current frequency (caused by the runtime), but also a Doppler frequency  $f_D$  (caused by the speed). Depending on the movement direction and the direction of the linear modulation, the radar after that measures only the sum or the difference between the difference frequency, as the carrier of the distance information, and the Doppler frequency, as a carrier of the velocity information. If the reflecting object moves towards the radar, then the frequency of the echo signal will be increased by the Doppler frequency. Now, if the measurement is made using a sawtooth signal, as it is shown in Figure 1.25, the Doppler frequency  $f_D$  is added to the difference frequency  $\Delta f$ . If the measurement is made using a falling edge of a sawtooth (equivalent to the mirror image of Figure 1.25), the Doppler frequency  $f_D$  is subtracted from the difference frequency  $\Delta f$ .

By choosing correctly the frequency deviation per unit of time, the radar resolution can be determined, and by choosing the duration of the increment of the frequency (the longer edge of the red sawtooth in Figure 1.25), the maximum non-ambiguous range can be determined. The maximum frequency

shift and steepness of the edge can be varied depending on the capabilities of the technology implemented circuit.

Signal bandwidth of FMCW-Radar can have values from 1 MHz up to 390 MHz. (Its upper border is mostly limited by legal reasons. For example, the mostly used border for FMCW-applications European ISM-radio band is defined from 24,000 MHz to 24,250 MHz with an established bandwidth of 250 MHz.) As the bandwidth increases, the achievable range resolution is decreasing, which means that the monitored objects can be seen in a more precisely way. The maximum detected range becomes smaller when the bandwidth increases. This can be shown in the table 1.1 [18]

| Bandwidth  | Range Resolution | Maximum Range | Required tx power | Example given                 |
|------------|------------------|---------------|-------------------|-------------------------------|
| 400 kHz    | 4,000 m          | 120 km        | 1,4 kW            | 76N6 (Clam Shell)             |
| 50 500 kHz | 1,500 100 m      | 15 250 km     | 30 W              | OTH oceanography radar WERA   |
| 1 MHz      | 150 m            | 75 km         | 1.4 4 kW          | Naval radar using a Magnetron |
| 2 MHz      | 75 m             | 37.5 km       | —                 | —                             |
| 10 MHz     | 5 m              | 7,500 m       | —                 | —                             |
| 50 MHz     | 3 m              | 500 m         | 4 mW              | DPR-886                       |
| 65 MHz     | 2.5 m            | 1,200 m       | 100 mW            | Broadband Radar TM            |
| 250 MHz    | 0.6 m            | 500 m         | 4 mW              | Skyradar Basic II             |
| 8 GHz      | 3.5 cm           | 9 m           | 4 mW              | Skyradar PRO                  |

**Table 1.1.** Relationship between bandwidth and other parameters.

As with any radar in the FMCW radar, besides the allocated bandwidth, the antenna beam-width determines the angular resolution in detecting objects, Figure 1.26.

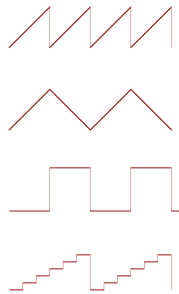


**Fig. 1.26.** Common modulation pattern for an FM-CW radar.

There are several possible modulation patterns, which can be used for different measurement purposes:

**Sawtooth modulation:**

This modulation pattern is used in a relatively large range (maximum distance) combined with a negligible influence of Doppler frequency (for example, a maritime navigation radar).

In a linear sawtooth frequency changing (Figure 1.25) a delay will shift the echo signal in time. This results in a frequency difference between the actual frequency and the delayed echo signal, which is a measure of the distance of the reflecting object. This frequency difference is called "beat frequency." An occurring Doppler frequency would now move the frequency of the entire echo signal either up (moving towards the radar) or down (moving away from the radar).

In this form of modulation, the receiver has no way to separate the two frequencies. Thus, the Doppler frequency will occur only as a measurement error in the distance calculation. In the choice of an optimum frequency sweep can be considered a priori, that the expected Doppler frequencies are as small as the resolution or at least, that the measurement error is as small as possible.

This will be the case for example in maritime navigation radar: Boats move in the coastal area at a limited speed, with respect to each other perhaps with a maximum of 10 meters per second. In this frequency band of these radar sets (XBand mostly), the expected maximum Doppler frequency is 666 Hz. If the radar signal processing uses a resolution in the kilohertz range per meter, this Doppler frequency is negligible. Because at an airfield occurring take-off and landing speeds of up to 200 m/s, a maritime navigation FM-CW radar would have trouble at all to see these planes. The measurement error caused by the Doppler frequency can be greater than the distance to be measured. The target signs would then theoretically appear in a negative distance, i.e. before the start of the deflection on the screen.

### Triangular modulation

In a triangular-shaped frequency changing, a distance measurement can be performed on both the rising and on the falling edge. In Figure 1.27, an echo signal is shifted due to the running time compared to the transmission signal to the right. Without a Doppler frequency, the amount of the frequency difference during the rising edge is equal to the measurement during the falling edge.

Doppler frequency shifts the echo signal in height (green graph in the figure 1.27). It appears the sum of the frequency difference  $\Delta f$  and the Doppler frequency  $f_D$  at the rising edge, and the difference between these two frequencies at the falling edge. This opens up the possibility of making a precise distance determination, despite the frequency shift caused by the Doppler frequency, which then consists of the arithmetic average of the two parts of measurements at different edges of the triangular pattern. At the same time, the precise Doppler frequency can be determined from two measurements. The difference between the two difference frequencies is twice the Doppler frequency. Since the two differential frequencies, however, are not simultaneously

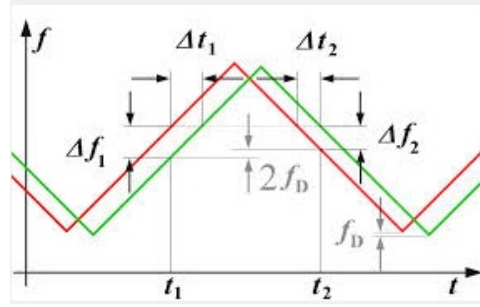


Fig. 1.27. Relationships with triangular modulation pattern.

available, this comparison requires digital signal processing, with intermediate storage of the measured results.

The Doppler frequency-adjusted frequency for the distance determination and the Doppler frequency of a moving target are calculated by:

$$f_{mess} = \frac{\Delta f_1 + \delta f_2}{2} \tag{1.60}$$

$$f_D = \frac{|\Delta f_1 - \delta f_2|}{2} \tag{1.61}$$

Being:

- $f_{mess}$  is the frequency as a measure of distance determination,
- $f_D$  is the Doppler frequency as a measure of the speed measurement,
- $\Delta f_1$  is the frequency difference at the rising edge and
- $\Delta f_2$  is the frequency difference at the falling edge

The frequency  $f_{mess}$  can then be used in the equation 1.59 to calculate the exact distance.

**Square-wave modulation (simple frequency-shift keying, FSK)**

This modulation is used for a very precise distance measurement at close range by phase comparison of the two echo signal frequencies. It has the disadvantage, that the echo signals from several targets cannot be separated from each other, and that this process enables only a small unambiguous measuring range.

**Stepped modulation (staircase voltage)**

This is used for interferometric measurements and expands the unambiguous measuring range.

**1.2.2.2 Signal Generation Through OFDM**

Orthogonal frequency division multiplexing (OFDM), a modulation scheme commonly utilized in commercial communications, shows a great potential

for use in forming radar waveforms. An OFDM signal is comprised of several orthogonal sub-carriers, which are simultaneously emitted over a single transmission path. Each sub-carrier occupies a small slice of the entire signal bandwidth. Technology advances helped in increasing the sampling speed capabilities, allowing accurate generation of Ultra Wide Band UWB-OFDM waveforms. This results in a diverse signal that is capable of high-resolution imaging. While OFDM has been elaborately studied and commercialized in the digital communication field, it has not yet been widely studied by the radar scientific community apart from a few efforts [5], [6]. The advantages of using OFDM in radar applications include: (a) Transceiver system is based on digital implementation using relatively inexpensive components (b) Ease of narrowband interference mitigation (c) High-resolution in UWB scale and good multi-path potential (d) Same architecture can be used to transmit large amounts of data in real time; and (e) Flexibility in pulse shaping using different sub-carrier compositions [19].

OFDM is a combination of modulation and multiplexing techniques, which allows the transmission of complex modulation symbols obtained through discrete phase modulation (e.g. BPSK) [20].

Then, OFDM modulation basically consists of combining  $n$  sub-carriers signals orthogonal to each other spaced in frequency by an  $\Delta f$  value, in order to obtain a single signal containing a bandwidth equal to  $n\Delta f$ .

The block diagram of the OFDM principle is schematically illustrated in Figure 1.28.

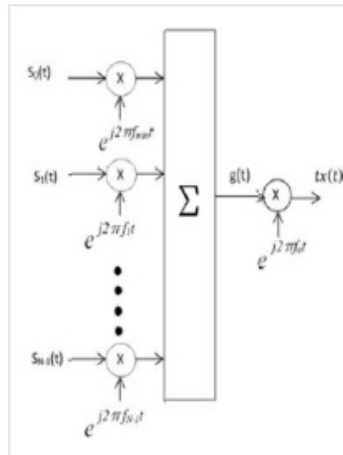


**Fig. 1.28.** Diagram of an OFDM Signal Generation. (Taken from [20])

The equation 1.62 shows the mathematical model to generate an OFDM signal starting from  $n$  sinusoidal signals, orthogonal among them.

$$g(t) = \sum_{k=0}^{N-1} S_k(t)e^{-j2\pi(f_{min}+k\Delta f)t} \tag{1.62}$$

Where:  
 $g(t)$  is the modulated signal with OFDM,  
 $k$  is the corresponding order of the orthogonal signal that will be added,  
 $N$  is the number of orthogonal signals,  
 $S_k(t)$  is a complex symbol (e.g. in BPSK it can be equal to 1 or -1 with duration  $T$ ),  
 $f_{min}$  is the minimum frequency with an arbitrary value ( it can be equal to 0)  
 $\Delta f$  is the frequency interval of spacing among the symbols. ( $\Delta f = \frac{1}{T}$ ) and  
 $t$  is the domain of the signal.

The Figure1.29 shows the generation of 4 sinusoidal signals, orthogonal among them as an example to combine them in one single OFDM signal.

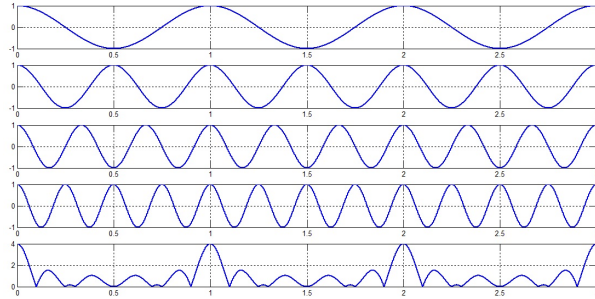


**Fig. 1.29.** OFDM Signal Generation.

Then, as it is seen in figure 1.28, it is necessary to modulate the signal to a carrier frequency that can be transmitted in the medium, obtaining the signal  $tx(t)$ .

Then from the equation 1.62:

$$tx(t) = g(t)e^{j2\pi f_c t} \tag{1.63}$$

Being:

$f_c$  is the carrier frequency to obtain the OFDM Signal.

OFDM radar works as a static system, by transmitting a signal of kind 1.63 and receiving reflections of this signal from objects in the path of the signal's wave front. It is important that transmitter and receiver are synchronized in order to avoid time or frequency offset [20]. The received signal, in absence of Doppler effect, can be expressed as:

$$rx(t) = \sum_{h=0}^{H-1} b_h g(t - \tau_h) e^{j2\pi f_c(t - \tau_h)} \quad (1.64)$$

Where:

$H$  is the number of reflecting targets,

$\tau_h$  represents the delay time of the corresponding signal caused by the distance  $d_h$  of every target and

$b_h$  is the attenuation for each target which depends on the material characteristics and the radar cross section.

The OFDM signal processing technique gives a maximum measurement distance defined as:

$$d_{max} = \frac{c}{2\Delta f} = \frac{Tc}{2} \quad (1.65)$$

Where  $c$  is speed of light.

The radar slant range resolution depends on the total bandwidth  $BW$  occupied by the transmitted signal, so it is given by:

$$\Delta_r = \frac{c}{2BW} = \frac{c}{2N\Delta f} \quad (1.66)$$

Figure 1.30 shows the block diagram for an OFDM radar, where the transmitted signal is composed by  $N$  symbols  $S = [S_0, S_1, S_2, \dots, S_{N-1}]^T$  modulated with  $N$  orthogonal frequencies  $f = [f_{min}, f_{min} + \Delta f, f_{min} + 2\Delta f, f_{min} + (N - 1)\Delta f]^T$  using OFDM technique. The total time  $T_t$  for an OFDM symbol considers the symbol duration  $T$  and a guard interval  $T_G$  [20], which is the time to avoid inter-symbol interference between subsequent OFDM symbols.

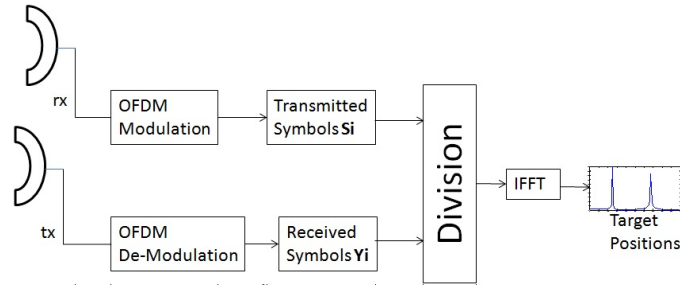


**Fig. 1.30.** OFDM Radar Block Diagram.

The received signal  $rx$  is demodulated, and a vector  $Y = [Y_0, Y_1, Y_2, Y_{N-1}]$ , containing the values of received symbols, is retrieved.

The target position is then obtained by applying the IFFT on the result of the wise division between the symbols received  $Y$  and the transmitted  $S$ .



### 1.2.3 OFDM Multi-band

In this work we have used the Modulation OFDM multi-band, which means to repeat the process explained in figure 1.28  $M$  times to different carrier frequencies, named  $f_{01}, f_{02}, \dots, f_{0M}$ . It generates  $M$  equal signals in different bands, being able to get results from the reaction of a dielectric material to the exposure of electromagnetic signals at various frequencies; then in figure 1.31 the scheme for generation of a OFDM multi-band signal is shown.

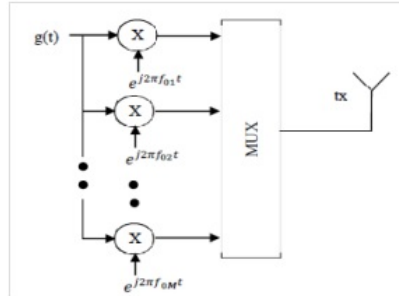


**Fig. 1.31.** OFDM Multi-band Generation. (Taken from [20])

There are two alternatives for obtaining an OFDM multiband signal  $tx$  [20]. The first one consists in transmitting all the OFDM waves at the same time, using only one shoot of  $T_t$  seconds, while in the second approach just one OFDM signal is transmitted each  $T_t$  seconds, with a total time signal of  $M * T_t$  seconds. The second option is the simplest one for processing and analysis, so it is adopted in this work where each band is multiplexed and sent one at a time, and later with the received data make to perform the appropriate processing to obtain the desired results.

In the figure 1.32 it is possible to see the distribution of the OFDM multi-bands along the spectrum in the frequency domain.

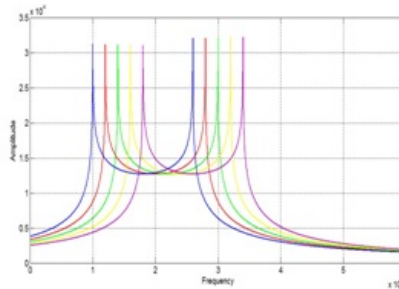


**Fig. 1.32.** Spectrum of OFDM multi-band signal

### 1.3 Scientific Background Research

As a previous study of these work, several tests and measurements were done, using instrument, devices and tools, that are properties of the  $\mu$ wave Lab of the UNICAL, which provides the equipment.

Among them, it is important to mention the NI USRP-2920 card universal software radio peripheral from the National Instruments.

#### 1.3.1 NI USRP-2920 Card Applications

USRP is an open-source project related to an electronic system for creating SDRadar applications. The USRP is the first device that can be interfaced with a PC through a software development tool-kit such as GNU Radio or Simulink, thus making possible the creation of different SDRadar applications. The first USRP motherboard was planned by Matt Ettus at the National Science Foundation in 2006 [22]. Nowadays, four versions are available: USRP, USRP2, USRP N200 and USRP N210. In the lasts years, the National Instruments has realized three new boards, namely USRP 2920, 2921, 2922 which interface with the PC through LabviewTM. Table 1.2 shows the main differences between the first-generation USRP and the last USRP NI 2920.

| USRP                                       | USRP NI 2920                        |
|--|-------------------------------------|
| GNU Radio or Matlab Simulink <sup>TM</sup> | Labview                             |
| 2 dual channel ACD converter at 64 MS/s    | 2 channels ADC, 400 MS/s            |
| 2 dual channel DAC converter at 128 MS/s   | 2 channels, 100 MS/s                |
| 1 USB 2.0 for PC interface                 | 1 Gigabit Ethernet for PC interface |
| 1 FPGA Altera Cyclone ( EP1C12 Q240C8)     | Xilinx Spartan-6                    |

**Table 1.2.** Software and hardware specification USRP Vs. USRP NI 2920

The NI USRP-2920 is basically a transceiver that operates in a band frequency from 50 MHz to 2.2 GHz. It is a peripheral device used in several fields of telecommunications above all in developing radio-frequencies field, research and implementation of wireless systems of communications correlated with SDR, Cognitive Radio and other digital system communications.

It is important to mention that the device is a low-cost solution above all in didactic and research applications.

This device permits the radio-frequency signal processing through a combined computational system that in this case is embedded inside of the device. In order to have an interface of control, processing and results, the LabView tool is used for these purposes.

The USRP card has a lot of potentialities [21] specifically in SDRadar, specially because of its ability to create multi-purpose radar, the ability to reuse hardware, the easy implementation of signal processing and the remarkable reduction of costs of production.

In particular, Zhang et al. propose in [23] a measurement system using a hybrid radar scheme with continuous wave frequency modulation and pseudo-random code pulse techniques. They show the ability to obtain high-precision information about the velocity of a vehicle, the distance, the direction and other information useful to improve the security in the automotive field. In [24], an experiment based on the usage of a SDRadar is conducted to implement a multifunctional software-defined unit well suited for radar sensor networks, which can be used for range measurements, radar imaging and data communications. It shows important results in order to highlight the issues and the limitations related to the combination of the SDRadar with radar systems. In [25], the capability of the USRP technology is demonstrated in the realization of a passive radar by designing a low-cost DVB-T software defined system for coastal ship detection, whilst in [26] an experiment is considered, which is based on the usage of a SDRadar to implement first a basic radar system and then a synthetic aperture radar, thus providing an advanced step towards the establishment of the concept of cognitive radar. More recently, the potential of SDRadar technology to obtain flexible and low-cost subsurface radar prototypes for the Ground Penetrating Radar (GPR) community, is investigated in [27], whilst a GNU Radio based software-defined Frequency Modulated-Continuous Wave (FMCW) radar, well suited for weather surveillance application, is implemented in [28] at a reduced cost and complexity. Fernandez et al. implement in [29] a SDRadar system able to transmit and receive chirp waveforms by using MATLAB and Simulink<sup>TM</sup> to implement the logic blocks, to process the received data and calculate the target range. The work in [30] presents a measurement testbed for OFDM radar which uses USRPs as a front-end. Since it requires little power, it can thus be easily installed in vehicles to perform measurements for car-to-car or car-to-infrastructure applications. Finally in [21] is proposed the implementation and testing of a low cost P-band SDRadar system for target detection by using a first-generation USRP programmed through Simulink as a reference approach, then extending the analysis to a new more powerful USRP 2920, produced by National Instruments (USRP NI2920), in order to obtain an increased resolution in target detection.

Most of the existing solutions discussed above are limited to assessing demonstrative SDRadar concept, thus a real compact SDRadar prototype is generally missed. As a matter of fact, in [23], [24], [27], [28] only laboratory experiments are performed, and standard instrumentations, such as signal generator, mixer and coupler, are adopted to simulate the SDRadar platform. A true USRP-based testbed is discussed in [30], but a low-range resolution is achieved, and a high direct coupling is produced, thus limiting the available dynamic range. In [25], a single preliminary experimental test is performed on a big ship, and the authors themselves declare to plane more experiments on smaller ships located at further distances, in order to give a reliable validation of the proposed approach. Furthermore, no verification of the radar range resolution is provided in [25]. In [26], the testing and configuration analysis of

the prototype is missed and declared in progress by the same authors. Finally, we can assert that in [21] a real USRP-based system is implemented achieving a great resolution with a high level of programmability and functionality.

### 1.3.2 Radar applied to Permittivity Measurement

Microwave pulses are used in radar and sonar to detect and locate targets in extended mediums. It can be used to find buried objects or voids by echo sounding, or can be used to probe snow fields or the depths of the earth. Although similar to radar in principle, there are important differences in these applications that can lead to significant variations in the design approach [31].

This kind of variations in the use of Radar Techniques, together to the advent of the computer and automatic test equipment, new techniques for measuring complex dielectric constant ( $\epsilon$ ) and permeability ( $\mu$ ) can be considered. Such a technique is described where a system is employed that automatically measures the complex reflection and transmission coefficients that result when a sample of material is inserted in wave guide or a TEM transmission line. Measurement results of  $\epsilon$  and  $\mu$  for two common materials are presented in [3] and [32].

When the electromagnetic energy reaches a discontinuity in the electromagnetic parameters of the medium, there is a physical phenomenon related to the interaction of the signal between a medium and the other, as in the transition zone, part of the signal is reflected and another is transmitted in the new medium of propagation, as is shown in figure 1.33.

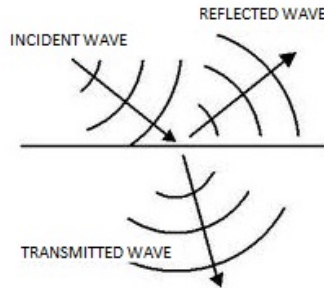


**Fig. 1.33.** Reflection of a wave in a medium change

This basically causes an attenuation in the reflected and transmitted wave since practically all the energy of the incident wave is divided proportionally at the resulting two waves when the signal undergoes changing the medium.

The percentage of energy reflected depends upon the contrast between the electromagnetic parameters of the different materials of the medium. This percentage is defined as the transmission and reflection coefficients of energy.

In the current study, an angle of incidence perpendicular to the sample to be characterized is considered, which implies working at normal incidence. Under these conditions, the coefficients of reflection and transmission only depend on the relationship between the electrical characteristics of the mediums, being the expressions of reflection and transmission coefficients as follows:

$$\Gamma = \frac{\sqrt{\varepsilon_1} - \sqrt{\varepsilon_2}}{\sqrt{\varepsilon_1} + \sqrt{\varepsilon_2}} \quad (1.67)$$

$$T = \frac{2\sqrt{\varepsilon_2}}{\sqrt{\varepsilon_1} + \sqrt{\varepsilon_2}} \quad (1.68)$$

It can be seen that the sum of the reflection coefficient (which represents the percentage of energy reflected in the incident energy) and the transmission coefficient (which represents the percentage of energy transmitted to the second medium, of the incident energy), is the unity. It can also be deduced from these equations that the reflectance is higher when the difference between the electromagnetic parameters of the mediums is larger, that means, that the greater contrast between the two mediums in contact, a greater percentage of the incident energy will be reflected at the discontinuity, and thus have a lower percentage of energy transmitted to the next medium; this theory is used as a part of characterization of a dielectric material exposed to a periodic electromagnetic signal using Radar devices.

Today there are several techniques to determine the permittivity of a dielectric using radar theory, but most of the information that exists is the use of GPR (Ground Penetrating Radar). That method is similar to the offset seismic reflection, but with the difference that it employees electromagnetic waves [33] that serve specifically to determine the permittivity of layers of the earth, working with samples that are larger than those expected for characterization of dielectric materials.

In [34] some techniques applied to permittivity measurement of a material using Radar Techniques are applied, some of them are listened here:

**Tabulated values:**

Used when the medium stratigraphy is known. In this case a complementary information is necessary, such as a geological exploration or a survey can provide. It basically consists in associating anomalies in the records of the boundary conditions of known materials. The thickness of every layer is obtained with the characteristic velocity of the wave along the materials that forming part of the layer.

**Geotechnical Models:**

These models are related to the relative permittivity of a medium with parameters as its composition, saturation and porosity. With these models is possible to plot the relative permittivity (for each medium composition) vs. the porosity and saturation.

**Stratigraphic information:**

Use the data of a near survey or other information about the sequence of medium materials, to compare the stratigraphy (materials and depth) with the anomalies of the records. It supposes the same depths that in the survey zone, and the velocities are calculated using the propagation double times registered with the radar.

**Static laboratory tests on soil samples of known thickness:**

It is necessary for a suitable sample's size for Radar measurements. Taking the propagation doubles times, the wave velocities are obtained.

**Reflection Coefficients:**

Base on the amplitude analysis. It comes to comparing the results obtained caused by the reflection in a medium surface with the obtained caused by a reflection in a metal sheet placed at the same distance of the sample in the first reflection. In the second case, a total reflection of energy is produced. If two resultant amplitudes are compared, in both cases, a comparison between an unitary reflection coefficient (in metal case) and reflection coefficient of the medium is done, that depends of effective permittivity of it. The principals troubles caused by this method are firstly that just there is direct information about the medium's surface and then there is not enough information of the medium's composition, and second, exists a little error in the amplitude measurements implies an important error in the permittivity resultant.

**Hyperbolas dynamic profiles caused by small objects in the medium:**

This is an applicable method, where does not exist an excessive error. This technique consists in determine the propagation velocity, calculating the hyperbola equation registered in the radar-gram. This equation depends of the depth where the reflector is placed (double vertical time of the reflection, known data), the position of the antenna on the surface according to the vertical axes of the element (known data), the double time of propagation registered in each point (known data) and the average velocity. A simple regression permits estimate a value for this velocity.

**CMP:**

It is a reliable method, but it needs a bi-static antenna. With this method the direct and refracted waves remain registered as a straight curve, while the reflections appear as hyperbolas. Using the hyperbola equation we have as in previous case the average velocity of propagation.

**Capacitance contrast:**

In a capacitor the capacitance between its plates is measured. Two measurements are done, first with air between the plates, and the other through the dielectric medium. It is an interesting method that provides a relative

permittivity, and it is the only one in the list that do not requires radar measurements to get the velocity of propagation.

In this work the method of the reflection coefficients is deepened since the technique developing, optimizing certain metrics and using the theory already mentioned above, is achieved the complex characterization of permittivity of a dielectric material on a scale of resolution smaller than used in the previously mentioned methods.





## Research Development

In the first chapter was discussed different techniques for material characterization and complex permittivity measurement. This chapter will describe the mathematical models obtained to determinate the values of complex permittivity of a dielectric, based on the theoretical approaches. The methodology used to obtain the measurements is also discussed as well the description of the electronic devices, software applied and the data processing.

### 2.1 Support Theory.

Several physic magnitudes and concepts were used to develop mathematical models, that are necessary for the dielectric characterization of a material. A detailed explanation of the characterization of the complex permittivity of a material using the irradiation of an electromagnetic signal is presented. In addition to this, the behavior of an electromagnetic signal propagated in a medium is exposed, as well as properties of Transmission and Reflection of a signal in different mediums of propagation. At the end of this section general concepts of the OFDM modulation are detailed.

#### 2.1.1 Complex Permittivity.

Absolute permittivity is the measure of the resistance that is encountered when forming an electric field in a medium. In other words, permittivity is a measure of how an electric field affects, and is affected by a dielectric medium. The permittivity of a medium describes how much electric field (more correctly, flux) is 'generated' per unit of charge in that medium. More electric flux exists in a medium with a low permittivity (per unit of charge) because of polarization effects. Permittivity is directly related to electric susceptibility, which is a measure of how easily a dielectric is polarized in response to an electric field. Thus, permittivity relates to a material's ability to resist an electric field and "permit" is a misnomer.

The electric displacement field  $D$  represents how an electric field  $E$  influences the organization of electric charges in a given medium, including charge migration and electric dipole reorientation. Its relation to permittivity in the very simple case of linear, homogeneous, isotropic materials with "instantaneous" response to changes in electric field is:

$$D = \varepsilon E \quad (2.1)$$

Where the permittivity  $\varepsilon$  is a scalar. If the medium is anisotropic, the permittivity is a second rank tensor.

In general, permittivity is not a constant because it can vary with the position in the medium, the frequency of the field applied, humidity, temperature, and other parameters. In a non-linear medium, the permittivity depends on the strength of the electric field. Permittivity as a function of frequency can take real or complex values.

In SI units, permittivity  $\varepsilon$  is measured in Farads per meter ( $F/m$ ); electric susceptibility  $\chi$  is dimensionless. These parameters are related to each other through:

$$\varepsilon = \varepsilon_r \varepsilon_0 = (1 + \chi) \varepsilon_0 \quad (2.2)$$

where  $\varepsilon_r$  is the relative permittivity of the material, and  $\varepsilon_0 = 8.8541878176... \times 10^{-12} F/m$  is the vacuum permittivity.

#### **Vacuum Permittivity:**

The vacuum permittivity  $\varepsilon_0$  (also called permittivity of free space or the electric constant) is the ratio  $D/E$  in free space. It also appears in the Coulomb force constant,  $k_e = \frac{1}{4\pi\varepsilon_0}$ .

Its value is:

$$\varepsilon_0 = \frac{1}{c^2 \mu_0} \approx 8.8541878176... \times 10^{-12} F/m \quad (2.3)$$

where  $c$  is the speed of light in free space and  $\mu_0$  is the vacuum permeability.

#### **Relative Permittivity:**

The linear permittivity of a homogeneous material is usually given relative to that of free space, as a relative permittivity  $\varepsilon_r$  (also called dielectric constant, although this sometimes refers only to the static, zero-frequency relative permittivity). In an anisotropic material, the relative permittivity may be a tensor, causing birefringence (Double Refraction). The actual permittivity is then calculated by multiplying the relative permittivity by  $\varepsilon_0$ :

$$\varepsilon = \varepsilon_r \varepsilon_0 = (1 + \chi) \varepsilon_0 \quad (2.4)$$

where  $\chi$  is the electric susceptibility of the material.

The susceptibility is the constant of proportionality (which is a tensor) relating an electric field  $E$  to the induced dielectric polarization density  $P$ :

$$P = \varepsilon_0 \chi E \quad (2.5)$$

The susceptibility of a medium is related to its relative permittivity  $\varepsilon_r$  by:

$$\chi = \varepsilon_r - 1 \quad (2.6)$$

So in the case of vacuum:

$$\chi = 0 \quad (2.7)$$

Also, the susceptibility is related to the polarizability of individual particles in the medium by the Clausius-Mossotti relation.

The electric displacement  $D$  is related to the polarization density  $P$  by:

$$D = \varepsilon_0 E + P = \varepsilon_0(1 + \chi)E = \varepsilon_r \varepsilon_0 E \quad (2.8)$$

The permittivity  $\varepsilon$  and permeability  $\mu$  of a medium together determine the phase velocity  $v = \frac{c}{n}$  of electromagnetic radiation through that medium:

$$\varepsilon \mu = \frac{1}{v^2} \quad (2.9)$$

### Complex Permittivity:

In contrast to the vacuum response, the response of normal materials to external fields depends on the frequency of the field. The fact that a material's polarization does not respond instantaneously to an applied field is demonstrated by the frequency dependence. The response must always be causal (arising after the applied field) which is represented by a phase difference. For this reason, permittivity is often treated as a complex function of the (angular) frequency of the applied field  $\omega : \varepsilon \rightarrow \hat{\varepsilon}(\omega)$  (since complex numbers allow specification of magnitude and phase). The definition of permittivity therefore becomes:

$$D_0 e^{-j\omega t} = \hat{\varepsilon}(\omega) E_0 e^{-j\omega t} \quad (2.10)$$

Where  $D_0$  and  $E_0$  are the amplitudes of the displacement and electric fields, respectively.

The response of a medium to static electric fields is described by the low-frequency limit of permittivity, also called the static permittivity  $\varepsilon_S$  (also  $\varepsilon_{DC}$ ):

$$\varepsilon_S = \lim_{\omega \rightarrow 0} \hat{\varepsilon}(\omega) \quad (2.11)$$

At the high-frequency limit, the complex permittivity is commonly referred to as  $\epsilon_\infty$ . At the plasma frequency and above, dielectrics behave as ideal metals, with electron gas behaviour. The static permittivity is a good approximation for alternating fields of low frequencies, and as the frequency increases a measurable phase difference  $\delta$  emerges between  $D$  and  $E$ . The frequency at which the phase shift becomes noticeable depends on temperature and the details of the medium. For moderate fields strength ( $E_0$ ),  $D$  and  $E$  remain proportional, and:

$$\hat{\epsilon} = \frac{D_0}{E_0} = |\epsilon|e^{j\delta} \tag{2.12}$$

Since the response of materials to alternating fields is characterized by a complex permittivity, it is natural to separate its real and imaginary parts, it is done by convention in the following way:

$$\hat{\epsilon}(\omega) = \epsilon'(\omega) + j\epsilon''(\omega) = \frac{D_0}{E_0}(\cos \delta + j \sin \delta) \tag{2.13}$$

Where:

$\epsilon'$  is the real part of the permittivity, it is related to the stored energy within the medium;

$\epsilon''$  is the imaginary part of the permittivity, it is related to the dissipation (or loss) of energy within the medium;

$\delta$  is the loss angle.

A dielectric permittivity spectrum over a wide range of frequencies is shown in Figure 2.1.  $\epsilon'$  and  $\epsilon''$  denote the real and the imaginary part of the permittivity, respectively. Various processes are labeled on the image: ionic and dipolar relaxation, and atomic and electronic resonances at higher energies.

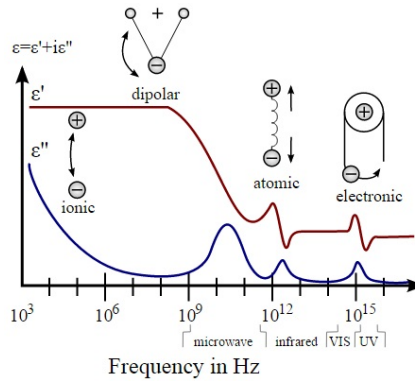


**Fig. 2.1.** Dielectric Permittivity spectrum over a wide range of frequencies.

The choice of sign for time-dependence,  $e^{-j\omega t}$ , dictates the sign convention for the imaginary part of permittivity. The signs used here correspond to those commonly used in physics, whereas for the engineering convention all imaginary quantities must be reversed.

The complex permittivity is usually a complicated function of frequency  $\omega$ , since it is a superimposed description of dispersion phenomena occurred at multiple frequencies. The dielectric function  $\varepsilon(\omega)$  must have poles only for frequencies with positive imaginary parts. Therefore the KramersKronig relations are satisfied. However, in the narrow frequency ranges that are often studied in practice, the permittivity can be approximated as frequency-independent or by model functions.

At a specific frequency, the imaginary part of  $\hat{\varepsilon}$  leads to absorption loss if it is positive (in the above sign convention) and a gain if it is negative. More generally, the imaginary parts of the eigenvalues of the anisotropic dielectric tensor must be considered.

In the case of solids, the complex dielectric function is intimately connected to band structure. The primary quantity that characterizes the electronic structure of any crystalline material is the probability of photon absorption. It is directly related to the imaginary part of the optical dielectric function  $\varepsilon(\omega)$ . The optical dielectric function is given by the fundamental expression: [45]

$$\varepsilon(\omega) = 1 + \frac{8\pi^2 e^2}{m^2} \sum_{c,v} \int W_{c,v}(E) [\varphi(\hbar\omega - E) - \varphi(\hbar\omega + E)] dx \quad (2.14)$$

In this expression,  $W_{c,v}(E)$  represents the product of the Brillouin zone-averaged transition probability at the energy  $E$  with the joint density of states, [46] [47]  $J_{c,v}(E)$ ;  $\varphi$  is a broadening function, representing the role of scattering in smearing out the energy levels [48]. In general, the broadening is intermediate between Lorentzian and Gaussian; [49] [50] for an alloy it is somewhat closer to Gaussian because of strong scattering from statistical fluctuations in the local composition on a nanometer scale.

### 2.1.2 Propagation in the mediums

Propagation medium is the space where the electromagnetic field moves along with certain amount of energy.

Each electromagnetic signal to be propagated responds differently in diverse mediums, and changes their properties such as the propagation speed, the attenuation suffered in traversing a medium, the signal offsets, among other parameters concerning the signal propagation. All these propagation characteristics, are linked to the electrical and magnetic properties of each of the medium, and it can be quantified with the magnetic permeability and electric permittivity of a medium.

Electromagnetic radiation is formed by the combination of electric and magnetic fields. Those are propagated through space in the form of carrier waves of energy. These electromagnetic waves are perpendicular vibrations in the direction of wave propagation. These are already perpendicular to each other, as it is shown in Figure 2.2. Therefore, they are classified among the transverse waves.

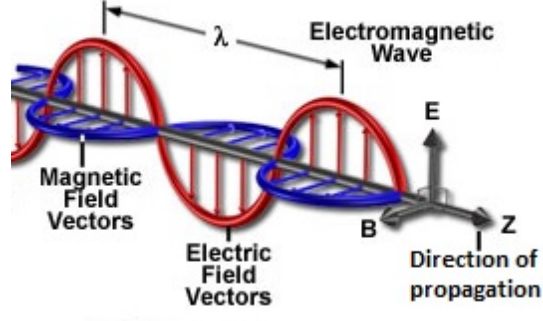


**Fig. 2.2.** Propagation of an Electromagnetic Wave

The behavior of these electromagnetic signals is summarized in four Maxwell equations in their most general form [7]:

$$\nabla \times E(r, t) = -\frac{\partial}{\partial t} B(r, t) \quad (2.15)$$

$$\nabla \times H(r, t) = \frac{\partial}{\partial t} D(r, t) + J(r, t) \quad (2.16)$$

$$\nabla \times B(r, t) = 0 \quad (2.17)$$

$$\nabla \times D(r, t) = \rho(r, t) \quad (2.18)$$

Where:

$E(r, t)$  is the Electric Field Intensity vector ( $V/m$ )

$H(r, t)$  is the Magnetic Field Intensity vector ( $A/m$ )

$D(r, t)$  is the Electric displacement vector ( $C/m^2$ )

$B(r, t)$  is the Magnetic flux density vector ( $W/m^2$  or  $T$ )

$J(r, t)$  is the Current density vector ( $A/m^2$ )

$\rho(r, t)$  is the volumetric charge density  $C/m^3$

$r$  is the position vector ( $m$ )

$t$  is the time ( $s$ )

So, solving these equations is possible to predict the behavior of the propagation of an electromagnetic signal in any medium, either in a vacuum, free space, dielectric materials, conductors, etc.; as well as in the boundary conditions between a material and another, where reflection, refraction and diffraction phenomena occur.

Considering a periodic electromagnetic signal it travels at the speed of light ( $c = 3 \times 10^8 m/s$ ) in vacuum or free space (air), but if the medium of propagation changes, the propagation speed decreases by:

$$v = \frac{c}{\sqrt{\epsilon'}} \quad (2.19)$$

The spread of a periodic signal  $f(t)$  in any medium is influenced according to the following relationship in time and distance:

$$f(r, t) = f(t)e^{-\gamma r} \quad (2.20)$$

Where  $\gamma = \alpha + j\beta$  is the propagation coefficient and as seen is a complex value where the real part represents the attenuation coefficient  $\alpha$  and the imaginary part is the phase coefficient  $\beta$ , and its value changes depending on the distance travelled by the wave in the propagation medium.

In this work we considered two conditions: the first one when the propagation medium is air and the second one when the medium is the dielectric material. In the first case the losses are not considered or are negligible ( $\alpha = 0$ ), therefore there is no attenuation; in the second case we consider the signal's attenuation caused by the dielectric material and in this case we use the model for low loss dielectrics:

$$\gamma = \frac{1}{2} \tan(\delta)\omega\sqrt{\mu\epsilon} + j\omega\sqrt{\mu\epsilon} \quad (2.21)$$

$$\alpha = \frac{1}{2} \tan(\delta)\omega\sqrt{\mu\epsilon} \quad \beta = \omega\sqrt{\mu\epsilon} \quad (2.22)$$

### 2.1.3 Transmission and Reflection of a signal in Materials.

When an electromagnetic signal is propagated in a medium such as vacuum and then it passes to another medium unexpectedly, the phenomena of transmission and reflection of the signal occurs, i.e., a part of the signal will be reflected back to the initial medium and the other will be transmitted to the new medium; each signal suffers property's changes, such as attenuation, phase change, decreased speed transmission, among others. To analyze each of these variations, there are some theories that allow examine the behavior of a signal when it changes from one medium to another, these theories are Snell's Law or Reflection Coefficients for plane waves.

Snell's law is a formula used to calculate the angle of refraction of an electromagnetic signal when it passes through the boundary between two propagation mediums with different refractive index.

It states that the multiplication of the refractive index by the sine of the angle of incidence is constant for any ray of light shining on the separation surface of two mediums. Although Snell's law was formulated to explain the phenomena of refraction of light, it can be applied to all types of waves through a surface between two mediums in which the propagation velocity of the wave varies.

Let's consider two mediums characterized by refractive indices  $\eta_1$  and  $\eta_2$  separated by a surface  $S$ . The signal rays passing through the two mediums will be refracted at the surface, this varies its propagation direction depending on the ratio between the refractive index  $\eta_1$  and  $\eta_2$ , as it is shown in Figure 2.3.

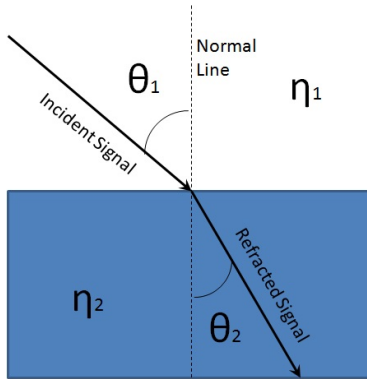


**Fig. 2.3.** Refracted Signal

$\eta_1$  and  $\eta_2$  are the refractive indices of the materials. The dashed line delimits the normal line, also defines when the signal changes from one medium to another. Snell besides refers to refraction, which is an imaginary line perpendicular to the surface. Angles  $\theta$  are the angles formed with the normal line, being  $\theta_1$  the angle of the incident wave and  $\theta_2$  the angle of the refracted wave.

For a signal with an incidence angle  $\theta_1$  on the first medium, the angle between the surface normal and the direction of propagation of the beam. The beam will propagate in the second medium at an angle of refraction  $\theta_2$  whose value is obtained by Snell's law.

$$\eta_1 \sin \theta_1 = \eta_2 \sin \theta_2 \quad (2.23)$$

Where the refractive constant  $\eta$  is the rate between the light speed in vacuum with the propagation velocity in a medium.

$$\eta = \frac{c}{v} \quad (2.24)$$



Note that in the case of  $\theta_1 = 0$  (incident ray perpendicular to the surface) the refracted rays emerge at an angle  $\theta_2 = 0$  for any  $\eta_1$  and  $\eta_2$ .

The symmetry of Snell's law implies that the paths of the signals are reversible. That is, if a ray incident on the interface at an angle of incidence  $\theta_1$  is refracted on the medium with a refractive angle  $\theta_2$ , then an incident beam in the opposite direction from the medium 2 with an incidence angle  $\theta_2$  is refracted on the medium 1 at an angle  $\theta_1$ .

A qualitative rule to determine the direction of the beam refraction is that the beam in the middle of higher refractive index is always close to the direction of the normal to the surface. The speed of light in the medium of higher refractive index is always smaller.

Plus to the Snell's Law, the reflection coefficient is another parameter that describes how much an electromagnetic wave is reflected by an impedance discontinuity in the propagation medium. The wave experiments partial transmittance and partial reflectance when the medium in which it travels changes suddenly. The reflection coefficient determines the ratio of the reflected wave amplitude related to the incident wave amplitude.

In particular, at a discontinuity in a transmission line, it is the complex ratio of the electric field strength of the reflected wave ( $E^-$ ) related to that of the incident wave ( $E^+$ ), and it can be written as:

$$\Gamma = \frac{E^-}{E^+} \quad (2.25)$$

On this study is considered a perpendicular incident angle with the sample to be characterized, it means working at normal incidence. Under these conditions, the coefficients of reflection and transmission only depend on the relationship between the electrical characteristics of the mediums. The expressions of reflection and transmission coefficients are as follows:

$$\Gamma = \frac{\sqrt{\varepsilon_1} - \sqrt{\varepsilon_2}}{\sqrt{\varepsilon_1} + \sqrt{\varepsilon_2}} \quad (2.26)$$

$$T = \frac{2\sqrt{\varepsilon_2}}{\sqrt{\varepsilon_1} + \sqrt{\varepsilon_2}} \quad (2.27)$$

It can be considered that the sum of the reflection coefficient (which represents the percentage of energy reflected to the incident energy) and the transmission coefficient (which represents the percentage of energy transmitted to the second medium, of the incident energy), is unity. And can be deduced from these equations that the larger the difference between the electromagnetic parameters of the mediums, the higher the reflectance is, that means, the greater the contrast between the two mediums in contact. A greater percentage of the incident energy will be reflected at the discontinuity, and thus have a lower percentage of energy transmitted to the next medium; this theory is used as part of characterization of a dielectric material exposed to a periodic electromagnetic signal.

## 2.2 Measurement Methodology.

Having explained the physical phenomena that suffers a dielectric when is irradiated by an electromagnetic signal and how it is generated and transmitted, in this section how these concepts are used to model the mathematical expressions will be explained; after completing the measurements this models will be used to process the data and to calculate the complex permittivity of the sample.

The technique used here for measurement is to use the reflections of a signal when it reaches a dielectric medium after being transmitted in free space, previously doing a calibration with PEC (Perfect Electric Conductor), yielding a complete reflection, which means that in the process two measurements are made on each band (18-23, 19-24, 20-25, 21- 26 GHz ) of OFDM signals, one directly to the PEC and the second placing the dielectric sample immediately before the PEC.

A scheme for the system is shown in figure 2.4

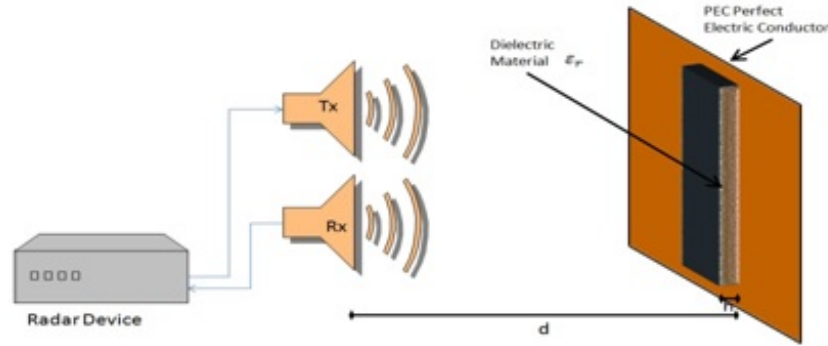


**Fig. 2.4.** System Scheme for Complex Permittivity Measurement

Then, as is possible to see in the figure 2.4 the PEC is placed at a distance  $d$  that can be known or not, because the system is capable of determining that distance and even the thickness  $h$ , depending on the resolution of the system. In this work an OFDM multi-band signal is used to accomplish a great resolution for measurement.

## 2.3 Mathematical Modelling

In this section the mathematical development employing physical concepts involved in the system is presented, it was used to obtain the mathematical models related to allowing the calculation of complex permittivity of a material exposed to the measurement.

Then, the signal considered to be transmitted is:

$$tx(t) = g(t)e^{j2\pi f_c t} \quad (2.28)$$

Being  $g(t)$  the OFDM signal, and the exponential part represents the modulation at a carrier frequency  $f_c$ .

In the first case, when the measurement is done directly toward the PEC without dielectric, the received signal after reflection is:

$$rx(t)_{cep} = -g(t - t_0)e^{j2\pi f_c t} e^{-\gamma z} \quad (2.29)$$

Where the negative sign represents complete reflection in the PEC (-1),  $t_0$  is the delay time of the signal having travelled from the transmitting antenna toward the PEC and returned to the source. And the exponent part  $e^{-\gamma z}$  represents the spread in this case in the free space, where  $\gamma = \alpha + j\beta$  is the propagation coefficient explained in a previous section and as was mentioned, the attenuation in this case is null thus  $\alpha = 0$ .

Developing the above expression the received signal is obtained, it is:

$$rx(t)_{cep} = -g(t - t_0)e^{j2\pi f_c (t - t_0)} \quad (2.30)$$

In the second case, the in presence of dielectric there are two signal contributions, i.e., there are two reflections, the first when the signal hits the dielectric sample, and the second when the signal crosses the dielectric hits the PEC and returns towards the source.

$$rx(t)_{diel} = rx(t)_{diel1} + rx(t)_{diel2} \quad (2.31)$$

The first reflection:

$$rx(t)_{diel1} = \Gamma_{12}g(t - t_1)e^{j2\pi f_c t} e^{-\gamma z} \quad (2.32)$$

Where  $\Gamma_{12}$  is the reflection coefficient at the transition free space - dielectric,  $t_1$  is the delay time employed by the signal in leaving the transmitting antenna, hit the dielectric and back to the source. And spread in this case is the same as in the previous case, therefore the development of this first equation is:

$$rx(t)_{diel1} = \Gamma_{12}g(t - t_1)e^{j2\pi f_c (t - t_1)} \quad (2.33)$$

The second reflection is given by:

$$rx(t)_{diel2} = -T_{12}T_{21}g(t - t_2)e^{j2\pi f_c t} e^{-\gamma z} \quad (2.34)$$

In this reflection are considered transmission coefficients when the signal makes transition between mediums in both directions ( $-T_{12}T_{21}$ ), there is also the time delay  $t_2$ ; but in this case there are two types of propagation in the mediums, one by each, i.e., in the free space where are not considered losses

and through the dielectric sample where the attenuation coefficient has a specific value ( $\alpha \neq 0$ ).

The product of the transmission coefficients can be developed as it follows:

$$T_{12} = (1 - \Gamma_{12}) \quad T_{21} = (1 - \Gamma_{21}) \quad (2.35)$$

$$\Gamma_{12} = -\Gamma_{21} \quad (2.36)$$

$$T_{12}T_{21} = (1 - \Gamma_{12})(1 + \Gamma_{12}) = (1 - \Gamma_{12}^2) \quad (2.37)$$

Then developing the transmission and reflection coefficients as well as the propagation coefficient, we have:

$$rx(t)_{diel2} = (1 - \Gamma_{12}^2)e^{-\alpha z} g(t - t_2)e^{j2\pi f_c t} e^{-j\beta z} \quad (2.38)$$

Where it was previously mentioned, in this contribution we had two mediums of propagation and their respective distances, in consequence, there is one different phase coefficient for each medium (equation 2.39). In the first medium (free space), the signal travels a distance of  $2(d - h)$  where  $d$  is the distance from the antenna to the PEC and  $h$  is the thickness of the dielectric material. In the second medium is considered just the thickness of the dielectric, that means a distance equal to  $2h$ .

$$\beta_1 = \frac{2\pi f_c}{c} \quad \beta_2 = \frac{2\pi f_c}{\frac{c}{\sqrt{\epsilon'}}} \quad (2.39)$$

Then:

$$rx(t)_{diel2} = (1 - \Gamma_{12}^2)e^{-\alpha z} g(t - t_2)e^{j2\pi f_c \left( t - \frac{2(d-h)}{c} - \frac{2h\sqrt{\epsilon'}}{c} \right)} \quad (2.40)$$

The distance travelled by the signal while it is attenuated inside the dielectric is  $z = 2h$  and  $t_2$  is the delay time of this reflection, thus:

$$rx(t)_{diel2} = (1 - \Gamma_{12}^2)e^{-2\alpha h} g(t - t_2)e^{j2\pi f_c (t - t_2)} \quad (2.41)$$

Being:

$$t_2 = \frac{2(d-h)}{c} + \frac{2h\sqrt{\epsilon'}}{c} \quad (2.42)$$

With the reflected and received signals is possible to do the data processing. It takes the existing attenuation caused by reflection and transmission coefficients, as well as losses in the signal propagation within the dielectric; time delays  $t_0$ ,  $t_1$  and  $t_2$  are also analysed, whereby it is possible to build a radargram where we can easily to determine the distance of each target

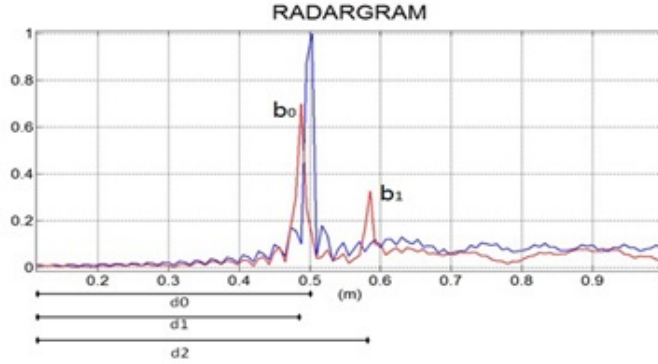


**Fig. 2.5.** Normalized Radargram of two measurements

reflection that is calculated using these delays when the signal travels at the speed of light.

The radargram of Figure 2.5 two signals are observed, the blue line represents the calibration, i.e., the measurement performed directly into the PEC without the presence of the dielectric, and the existing peak at a distance  $d_0$  caused by the delay time  $t_0$  represents the distance from the antennas until the PEC, as can be seen both signals are normalized to this reflection.

The red line represents the measurement made when the sample dielectric is placed before the PEC. Two peaks are observed, the first one is located at a distance  $d_1$  caused by the delay  $t_1$  represents the distance from the antenna to the dielectric, and the second peak located at a distance  $d_2$  caused by time  $t_2$  represents the signal reflection against the PEC after passing through the dielectric.

Distances  $d_0$  and  $d_1$  are real distances because the entire route traveled by the signal is in free space and the analysis performed for the radargram is assuming the speed of light ( $c = 3 \times 10^8$ ).

$$d_0 = \frac{t_0 c}{2} \quad d_1 = \frac{t_1 c}{2} \tag{2.43}$$

$d_2$  is instead a fake distance because when the signal crosses the dielectric section, the signal travels at a slower speed than the speed of light  $v = \frac{c}{\sqrt{\epsilon'}}$

$$d_2 = \frac{t_2 c}{2} \tag{2.44}$$

Then, the equality of  $t_2$  in equation 2.42 is applied, the distance  $d$  is the same distance  $d_0$  that appears in the radargram and knowing that  $d_1 = d_0 - h$  we have:

$$t_2 = \frac{2(d_0 - h)}{c} + \frac{2h\sqrt{\epsilon'}}$$

$$= t_1 + \frac{2h\sqrt{\epsilon'}}$$
(2.45)

Developing:

$$\frac{2d_2}{c} = \frac{2d_1}{c} + \frac{2(d_0 - d_1)\sqrt{\epsilon'}}{c} \quad (2.46)$$

Finally clearing the value of the real permittivity the next equation is obtained:

$$\sqrt{\epsilon'} = \frac{d_2 - d_1}{d_0 - d_1} \quad (2.47)$$

It is possible to calculate the value of the real part of the permittivity only with the distances in the radargram of Figure 2.5.

To finally obtain the loss tangent, an attenuation analysis is done. It is necessary to process the obtained and normalized amplitudes acquired in the Figure 2.5 ( $b_0$  and  $b_1$ ), which basically represents the attenuation expressed in the equations 2.33 and 2.41 for each contribution received at her reflection in the measurement with presence of the dielectric.

$$b_0 = \Gamma_{12} \quad b_1 = (1 - \Gamma_{12}^2)e^{-2\alpha h} \quad (2.48)$$

Thus:

$$b_1 = (1 - b_0^2)e^{-2\alpha h} \quad (2.49)$$

Hence, using the equation 2.22 for the attenuation coefficient in dielectric mediums with losses, we may develop the equation 2.49 and obtain the value of the loss tangent:

$$\tan(\delta) = \frac{c}{2\pi f_c h \sqrt{\epsilon'}} \ln \left( \frac{b_1}{1 - b_0^2} \right) \quad (2.50)$$

Thereby obtaining the complex permittivity of a dielectric material through the delay time that this causes, as well as the attenuation when passing through it.

## 2.4 Equipment and devices used.

The instruments, tools and devices used for the development of this work have been selected according to the needs of signal generation, so has required a high-frequency OFDM modulator (Anritsu 37269C Vector Network Analyzer) to optimize the available bandwidth, Antennas Horn (TX and RX) suitable for operation at the frequencies (Millimeter Products INC. 261K 595 Standard Gain Horns); tests and measurements have been performed within an Anechoic Chamber in the *μWaveLab* of the UNICAL while the data obtained processing has been performed on a high performance computer using Matlab.

A brief description of the devices and tools used in the preparation of this measurement system is presented.

### 2.4.1 Anritsu 37269C Vector Network Analyzer, 40 MHz to 40 GHz

The Anritsu 37269C Vector Network Analyzer (VNA) is a high performance tool designed to make fast and accurate S-parameter measurements of passive devices across the 40 MHz to 40 GHz range. The Anritsu 37269C Vector Network Analyzer (VNA) integrates a synthesized source, S-parameter test set and tuned receiver into a single compact package that is ideal for bench-top testing. High throughput measurements are achieved through the use of fast, 12-term error corrected sweeps, fast GPIB data transfers and an intuitive user interface. All measurement results are displayed on a large LCD color display on an external VGA monitor.

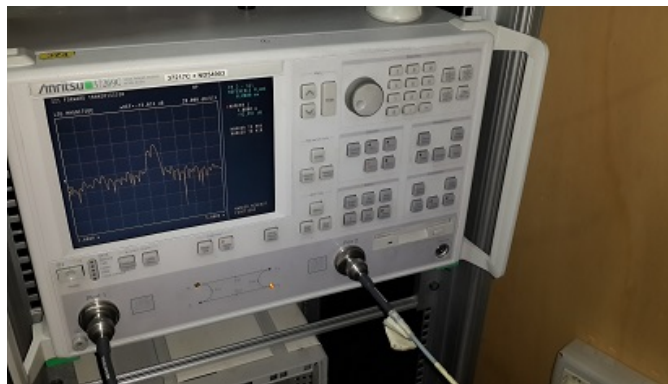


**Fig. 2.6.** Anritsu 37269C Vector Network Analyzer

#### **Features:**

- Fast Sweeping Synthesized Source
- Four Independent Display Channels
- Multiple Source Control of Two External Sources
- Four Channel Receiver
- Internal Hard and Floppy Disk Drives
- LRL/LRM Calibration
- Adapter Removal Calibrations
- Fast Measurement Throughput via GPIB
- Built-In AutoCal Control

### 2.4.2 Millimeter Products INC. 261K 595 Standard Gain Horns

Mi-Waves 261 series standard gain horns are fabricated with very close tolerances to ensure the precision of every horn manufactured by Mi-Wave. Each unit is joined to a short section of rectangular wave-guide and terminated in a standard flange.

Standard gain horns can be used to determine experimentally the gain of other antennas by using the substitution method. The standard gain horn and the antenna under test are alternately connected to a well-matched detector system in order to compare their relative power levels. The power level difference is then added to the appropriate level of the calibration curve to determine the absolute gain of the antenna under test.

Standard gain horns are also useful as power monitors in radar transmitter tests as is the case of this thesis, known-gain radiators in field propagation studies, and transmitting or receiving antennas in test bench applications. The completed units are gold-plated to protect from corrosion and for minimum RF losses.

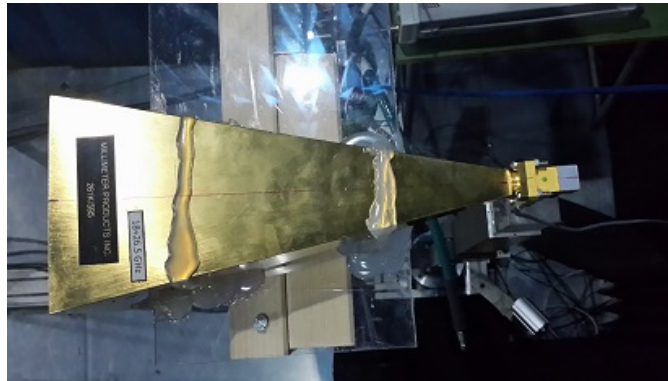


**Fig. 2.7.** 261K 595 Standard Gain Horn.

**Features:**

Nominal Gain of 25 dBi

Available from 12.4 to 220 GHz

Made with Precise Dimensional Tolerance Control

Gain Calibration is Accurate to 0.5 dB Over Full Wave-guide Bandwidth

Other Gain Values Available upon Request, ex: 10, 15, 20, etc.

### 2.4.3 Anechoic Chamber of the $\mu$ WaveLab UNICAL

Microwave Laboratory of UNICAL ( *$\mu$ WaveLab*) has built over the years a remarkable capacity for solutions to the problematic related to simulation, design, construction and measurement of microwave components and antennas. The laboratory has participated in projects with the antenna purposes and its applications in collaboration with various business entities, consortia development and research partnerships, developing and designing prototypes of new antennas and measurements corresponding to parameters and components.





**Fig. 2.8.** *μWaveLab* Logo

In this lab works since May 2010 the anechoic chamber of average dimension, it is shown in the figure 2.9, this camera has innovative features for flexible mode, measurements of electromagnetic diffusion and characterization of antennas and materials.

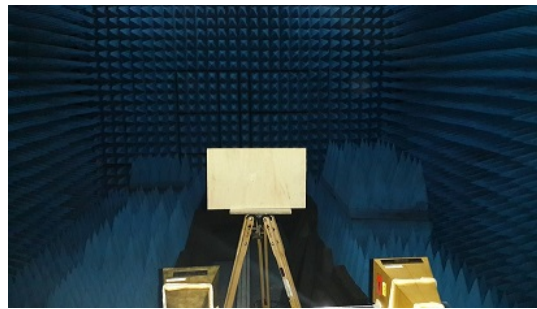


**Fig. 2.9.** Inside the Anechoic Chamber

The chamber dimensions are 8.5m x 6m x 5.5m and are fully shielded with a 2mm. laminate. The Internal anechoic is coated with 18" panels (Figure 2.9).

The Entrance to the Chamber is through a side door. There are also two further openings: A small access in the area near the planar scanner for any external probes and a semi-fixed opening comprising most of the wall opposite the scanner, in order to introduce into the chamber large objects. In the Chamber is possible to make characterization measurements into either near-field and far-field. A rail travels throughout the chamber, carrying a trolley with plexiglass stand with adjustable height. The Planar Scanner that is in front of the small chamber wall is large 5m. x 4.2m.

The displacement system uses Brushless motors controlled by an AC servo drive and managed from a National Motion Control Step 5 card. Management software developed in LabView, is very flexible, allowing not only making acquisitions of canonical surfaces scansions, but also on strategic and innovative geometries. The control system is integrated to the acquisition of data from a Network Analyzer. The extreme flexibility of the software allows for example the simultaneous acquisition of a set number of frequencies, scansions with non-homogeneous sampling, scansions on polygonal surfaces etc.

Inside of the anechoic chamber there are four cameras, which allow continuously monitor the development of the measurements (Figure 2.10).



Fig. 2.10. Monitoring System

## 2.5 Information Processing

As mentioned previously, the information collected in the measurements, is processed in an algorithm developed in Matlab, where the data initially is received in a text file with extension .txt, in which the general information about the configuration of the signal generator device is displayed together with the real data of received signal. This data includes the number of points, the distance in centimeters scale and the amplitude in dBs scale, as it is shown in Figure 2.11.

```

DIC1924P - Blocco note
File Modifica Formato Visualizza ?
37269C
MODEL: DATE: 07/16/2014 17:25 Page 1
DEVICE ID: OPERATOR:
START: 19.000000 GHz GATE START: 1.0000 cm ERROR CORR: 12-TERM
STOP: 24.000000 GHz GATE STOP: 2.0000 cm AVERAGING: 1 PT
STEP: 0.003125 GHz GATE NOMINAL IF BANDWIDTH: 1 KHz
WINDOW: NOMINAL
PARAMETER: ---CH3--- -S21-
NORMALIZATION: OFF
REFERENCE PLANE: 0.0000mm
SMOOTHING: 0.0 PERCENT
DELAY APERTURE: -
PROCESSING: DISTANCE
GATING: OFF
MARKERS:
MKR DISTANCE MAGNITUDE
# cm dB
1 1.0000E+02 -85.060
DISTANCE POINTS:
PNT DISTANCE MAGNITUDE
# cm dB
1 2.0000E+02 -85.060
2 2.0019E+02 -84.204
3 2.0037E+02 -83.637
4 2.0056E+02 -83.047
5 2.0075E+02 -82.525
6 2.0094E+02 -82.062
7 2.0112E+02 -81.652
8 2.0131E+02 -81.291
    
```

Fig. 2.11. Received Signal in a TXT File

Then, before to use these data it is necessary to modify the file and to keep only the columns of the distance and amplitude, eliminating everything else, thus importing the file to Matlab as a .mat file in which every column is considered as a data vector, in this way the information can be manipulated easily.

Finally, having the two received signals processed, both the calibration with the PEC as with dielectric located before the PEC, they are used in the algorithm in Matlab, where the equations 2.47 and 2.50 are applied.



## Results and Discussion

The following chapter discourses the measurements, data collection, and data validation in detail as well as the verification of results, and the comparison with other techniques. The data collection of experiments comes from the measurements in the anechoic chamber, located at the University of Calabria, with a vector network analyser by varying the frequency bands (18 - 23, 19 - 24, 20 - 25, 21 - 26 GHz ) to obtain the variation of permittivity versus frequency. Implementing a Matlab script the data collected is processed and the results are showing.

Finally, a general performance balance is presented, showing the advantages to using the method that calculate the Complex Permittivity described in this thesis

### 3.1 Data Collection.

A piece of wood was used as a dielectric material, whose permittivity is known [7], it allows to compare the theoretical values with the measured values.

Figure 3.1 shows a detailed system scheme, where all the devices and components mentioned in the preceding chapter were shown.

As it was explained in the previous chapter, the methodology measurement process has two stages: the first one, directly to a PEC placed at a specific distance from the antenna (Figure 3.2), where the signal generated is radiated. This signal impacts the PEC, and then it is received by the antenna and stored in a text file in the vector analyser.

After, the same process is repeated, but placing now the dielectric sample before the PEC (Figure 3.3). In this case has been used as a sample of dielectric material a piece of wood, the value of complex electrical permittivity is known [7], for consecutively compare values and demonstrate the proper performance of this work, and another text filed is generated and stored in the vector analyser.

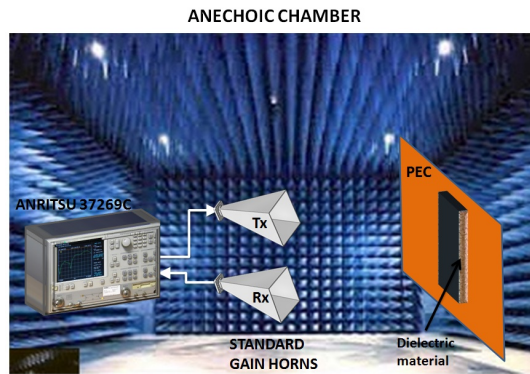


Fig. 3.1. Detailed Scheme of the measurement system

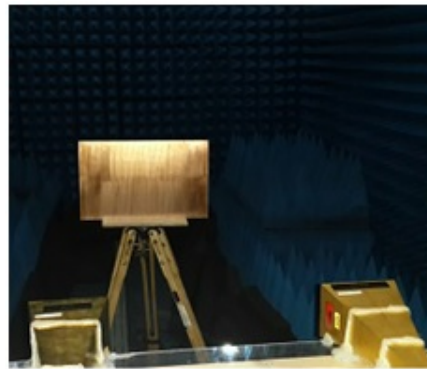


Fig. 3.2. Calibration Measurement (Directly to the PEC)

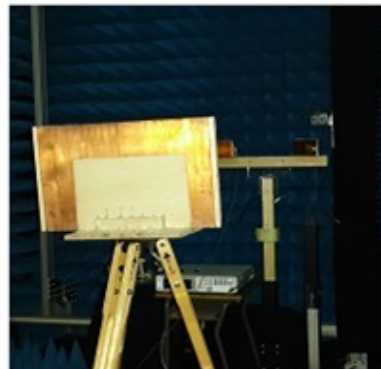


Fig. 3.3. Dielectric Measurement

The obtained text files generated for each measurement are processed and modified. Thus, this files can be used in the Matlab script. At the beginning of this process, each text file has a header with information about the settings of the vector network analyser (Figure 2.11), all of this information is removed and just is kept the column with the necessary data information of the received signals. This process scheme is shown in figure 3.4 and Figure 3.5 shows an example of the resulting file. These new files are used to perform the proper processing algorithm designed in Matlab.

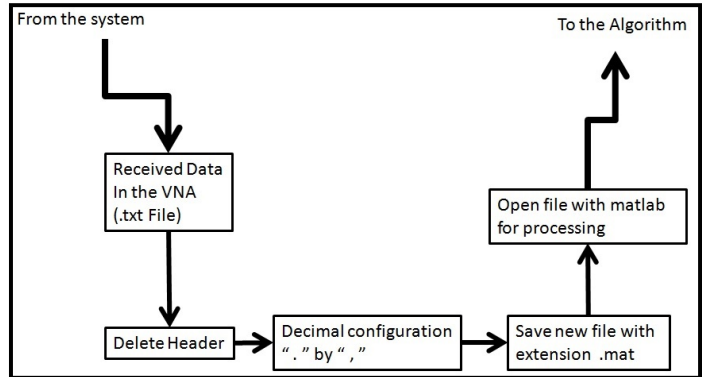


Fig. 3.4. Text Processing from the .txt file received in the VNA to the .mat file, used in the Algorithm in Matlab

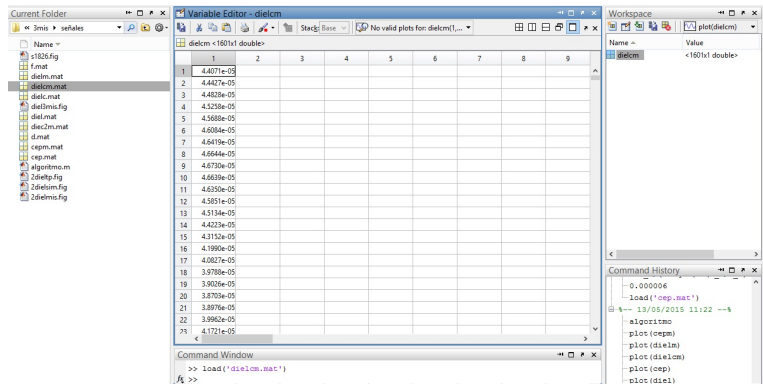


Fig. 3.5. File .mat of a received signal just with necessary information

### 3.2 Data validation and method evaluation.

Once the data is collected and stored, it is necessary to process it by using an algorithm implemented in a Matlab script to built the radargrams of each signal, i.e. the signal received at the calibration measurement made directly in the PEC and signal received when the dielectric material is placed before the PEC.

The algorithm is detailed in a brief diagram shown in figure 3.6

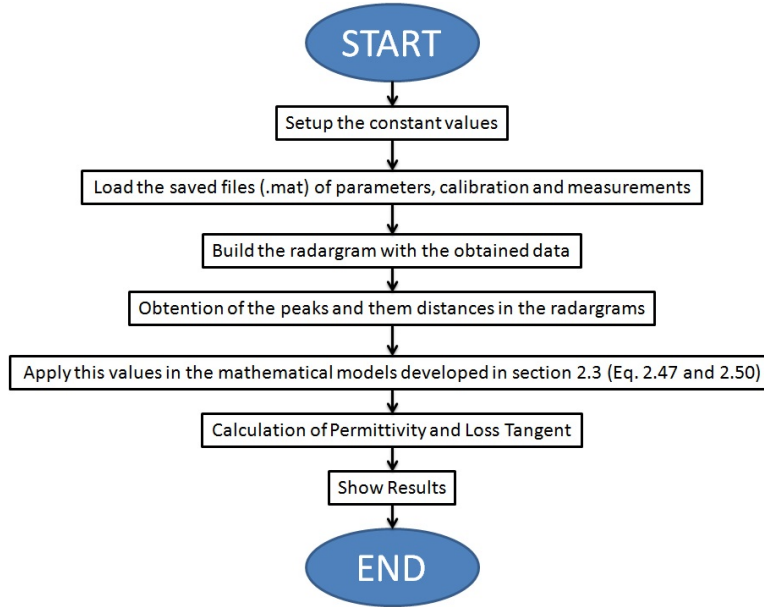


Fig. 3.6. Brief diagram of the algorithm in matlab

Following the procedure of the Figure 3.6, the radargrams obtained in each measurement are compared with those obtained in the simulation step.

#### 3.2.1 Measuring Simulation System

A Matlab script simulates the behaviour of the system measuring, in which has a reference point and control over the received signals.

The simulation algorithm considers all the steps of the process: The signal generation, transmission, calibration (with a complete reflection in the PEC), measurement (considering partial reflection and signal attenuation when the signal passes through the dielectric material), and the delay in each measurement. This Matlab script uses the values of permittivity and loss tangent of the material from the literature.



The obtained results after the simulation are the radargrams of reflected and received signals, as the Figure 3.7 shows.

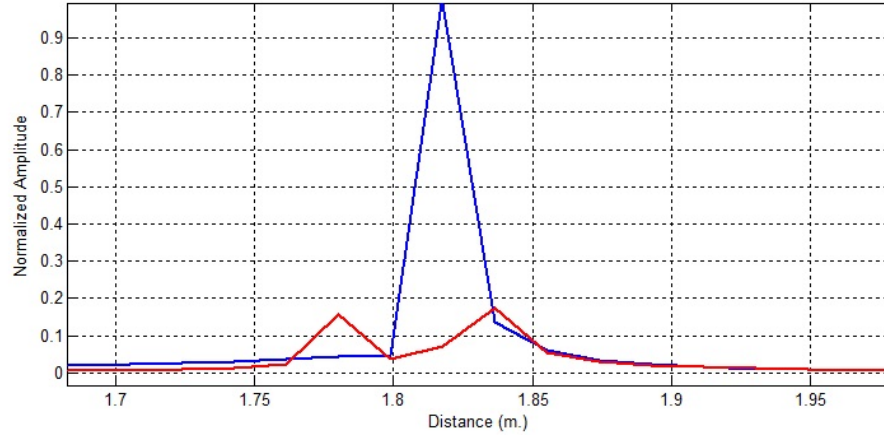


**Fig. 3.7.** Simulation permittivity measurement system

The radargram shows the calibration signal using only the PEC (blue line) and the measurement signal with the dielectric material placed (red line).

Therefore the measurements should necessarily be similar to those obtained in the simulations, to prove the proper functioning of the algorithm, which processes the received signals and obtains the expected results.

### 3.2.2 Making several measurements

After the simulations, with the corresponding parameters and conditions involved in measurements (Value of the complex permittivity of the sample, distance from the antenna to the sample, sample thickness, signal generated, etc). We compare the measurements with the simulation results, as Figure 3.8 shows. The results are similar to the data obtained in the simulation (Figure 3.7). This comparison shows the proper operation of data collection and its processing.

But, to verify the correct performance of the system, several measurements using different materials were done.

Then, as mentioned above, with the values obtained in peaks of radargrams and applying the expressions in the Matlab script, the values of permittivity and loss tangent (frequency dependent values) are obtained.

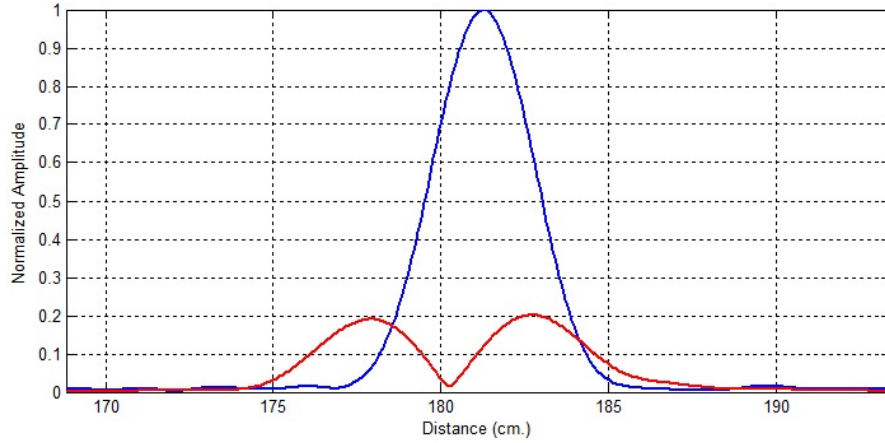


Fig. 3.8. Radargram obtained from Measurements

### 3.2.3 Comparison of results with known values

The results of the measurements were validated with simulations and compared with theoretical values from the literature, [7], [51] [55], ensuring the proper performance of the system.

Figure 3.9 shows the values of the relative permittivity and loss tangent of materials used for the measurements, these values are related to frequency.

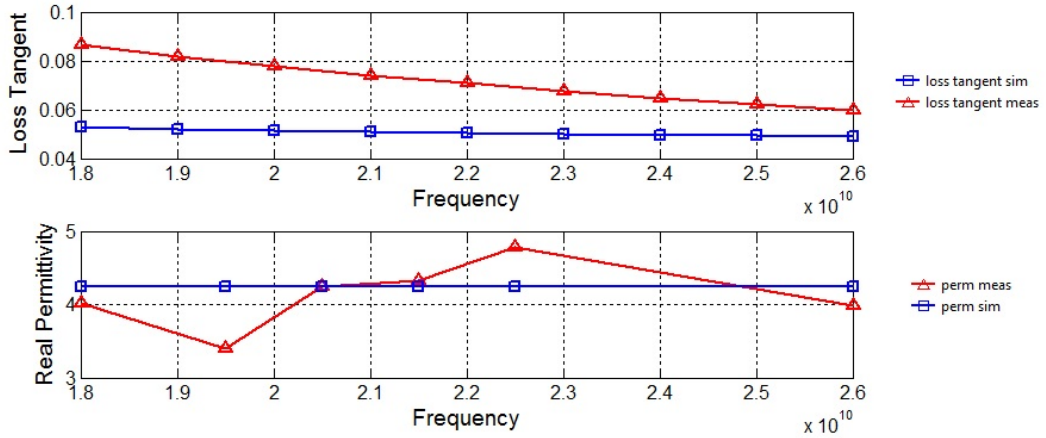


Fig. 3.9. Relative Permittivity and Loss Tangent of wood sample.

The red lines represent the values obtained in the measurements, and blue lines are the theoretic values of the wood permittivity, according to their elec-

trical behaviour against an electromagnetic signal over a range of frequencies defined under normal conditions.

Using the SDRadar techniques and optimizing the usage of the electromagnetic spectrum with multiband OFDM signal generation, the results collected were close to the theoretical ones, whereby the proper performance of the system and the mathematical models obtained were tested.

In this case, we use samples of wood as a dielectric material, the results are shown in Table 3.1, where the values are compared with the media of known values, taken from the bibliography, [7], [53], [55].

| Wood            | Real Permittivity | Loss Tangent |
|-----------------|-------------------|--------------|
| Known Values    | 2 - 6             | 0.05 - 0.07  |
| Measured Values | 3.2 - 4.8         | 0.06 - 0.082 |

**Table 3.1.** Comparison between known values and measured values of real Permittivity and Loss tangent of wood.

### 3.3 Comparison with similar techniques.

As it was mentioned in the Chapter 1, there are several techniques for complex dielectric characterization of materials. In between them, the contact method and free space method were mentioned.

The comparison of these techniques evaluates the performance of our system, and the correct development of the models used in the algorithm.

The variations can be caused by the environment of the measurement, due to the temperature, humidity and type of materials. This variation can change in all measure conditions. And as it is known, the complex permittivity value varies with those physic conditions. The maximum value obtained, of difference between our method and the other techniques is estimated to be within  $\pm 8\%$ .

### 3.4 Advantages of using this technique.

There are many advantages of this type of characterization, and the list of this advantages starts from it is an application of SDRadar. The properties and the configuration of this technique are adaptable to the measured system and end with the cost reduction in the implementation of this system using only one SDRadar device.

With this technique developed for Material Characterization, it is possible to obtain not only the real value of permittivity  $\epsilon'$  as in the simple methods, but the complex value:

$$\varepsilon = \varepsilon' + j\varepsilon'' \quad (3.1)$$

The imaginary permittivity value strongly depends on the loss tangent  $\tan(\delta)$ , that is one of the values obtained with this applied technique.

Furthermore, the possibility of parameters modification involved in the measurement is other of the advantage of this novel method, for example, the system allows to add new variables, such as the temperature of the medium, humidity, size of the sample, among others. It allows perform measurements in different environments conditions, just by doing simple changes in the settings configuration of the script.

By varying the algorithm, it is possible to obtain other parameters in the sample, which depend on the permittivity, such as Transmission or Reflection Coefficients, Conductivity, Phase coefficient and Attenuation coefficient.

The resolution obtained with this technique reaches an optimal value of 1,6 millimetres, due to the way the signal generation and its bandwidth (18 - 26 GHz). With this resolution, it is possible to perform measurements more accurate. The separations between the possible peaks are smaller, and this helps the calculation in the algorithm execution described in section 2.5.

The preparation of the sample to measure is simple because it is necessary only a plate of the dielectric material to characterize with a thickness of at least the minimum value of resolution, ( $h > 1.6mm$ ), and then it can proceed with the methodology described in section 2.2.

This method is designed for measurements in solids, but it could be possible to do the measurements to liquids just changing the antenna's position. Instead of put them in a horizontal way, for creating a normal radiation to the sample, it should be placed in a vertical position, so that the electromagnetic waves travel toward the liquid sample placed in a container with a metallic background, and the radiation will be normal. That means to use the same system only turned 90 degrees.

## Conclusions

To conclude this thesis, the conclusions, suggestions, and future work is discussed, and the more remarkable issues and more relevant topics are summarised.

### 4.1 Conclusions.

The use of a radar system has been proposed in this work to characterize a dielectric material by recovering the value of the relative electrical permittivity and tangent loss. The theory of reflection and multireflection has been used to develop an approach, which provides a simple but accurate prediction of the dielectric parameters.

A simple, low-cost with acceptable accuracy technique for measuring the material complex permittivity was designed and implemented in this work. This technique is based on measuring the amplitude of transmission/reflection coefficients in presence of the material sample to do permittivity measurement after solving the measured data numerically. The numerical solution was achieved in this work with the assistance of a script implemented in Matlab.

The proposed characterization method is particularly suitable to analyse dielectric materials at microwave frequencies. Good results can be achieved if the material sample width is greater than the minimal resolution supported by the system by more than three times to reduce the effect of the multireflections.

The main advantage of this technique is no need for a guess or approximate value of the sample permittivity, as in a short-circuited line technique where infinite solutions exist, which makes the solution a unique.

The use of SDRadar techniques has proved to be an interesting solution for many applications related to the reflected waves against a target and the characterization of this element.

The calibration of the system (using only the PEC) is a very important step to the good performance of the measurements.

The mathematical models obtained and applied in the algorithm have been developed correctly, and tested so that the results are accurate.

## 4.2 Suggestions

As in every work developed, always there are little things that could be improved, such as to have a larger number of materials to validate the method of characterization, or to improve the resolution with a better bandwidth.

One of the most important suggestion is the fact that the measurements must be done in a clean environment, free of perturbation, or interference or another sources. For that reason is advisable to do the measurements in an anechoic chamber as well as the measurements were done in this work, to avoid getting erroneous data in the collection of information.

The system calibration plays a very crucial roll in the development of the measurement. Thus an appropriate PEC must be chosen, like a cooper plate or some metal that implies a total reflection of the transmitted signal.

## 4.3 Future Work

One of the principal objectives of this P.H.D. is to continue the research work and develop the actual applications in my origin country Ecuador. For this reason, some of the most important things to do when I return and I belong to a group of applied research are:

- Implement this system in the research centres in Ecuador to develop this kind of applications.

- Provide the tools, services and facilities in the research centres to make the correct measurements in a suitable way.

- Make other measurements with other materials that values can be known or unknown.

- Build a system in which it could be possible to make measurements with changes of temperature of the sample and to obtain results of complex permittivity in function of the temperature.

- Explore the possibility of research centres offer services to enterprises and companies, which have been developed in this thesis.

---

## References

1. Ing. JUAN FERNANDO CORONEL RICO, "Estudio y caracterizacin de ecos de radar de onda continua aplicados a la medicion de nivel de fluidos homogeneos y heterogeneos", Tesis para el grado de Magister en Ingeniera Elctrica, Universidad Nacional de Colombia, Bogota, Colombia 2011. Available from: <http://www.bdigital.unal.edu.co/6434/1/300045.2012.pdf>
2. Wan, Changhua ; Nauwelaers, B. ; De Raedt, W. ; Van Rossum, Marc, "Two new measurement methods for explicit determination of complex permittivity", Microwave Theory and Techniques, IEEE Transactions on (Volume:46 , Issue: 11 ), p. 1614-1619, November 1998.
3. Ghodgaonkar, D.K. ; Dept. of Eng. Sci., Pennsylvania State Univ., University Park, PA, USA ; Varadan, V.V. ; Varadan, Vijay K. "A free-space method for measurement of dielectric constants and loss tangents at microwave frequencies", Instrumentation and Measurement, IEEE Transactions on (Volume:38 , Issue: 3 ), p. 789 - 793, June 1989.
4. Eduardo Nebot del Busto "Caracterizacin de dielctricos a frecuencia de microondas." Memoria presentada para la evaluacin de trabajo academicamente dirigido, Universidad de Zaragoza Facultad de Ciencias Departamento de Fisica Aplicada area de Electromagnetismo, Zaragoza, Spain, July 5 2004. Available from: [http://www.unizar.es/departamentos/fisica\\_aplicada/tads/TAD%20Eduardo.pdf](http://www.unizar.es/departamentos/fisica_aplicada/tads/TAD%20Eduardo.pdf)
5. Garmatyuk, D. ; Miami Univ., Oxford ; Schuerger, J. ; Morton, Y.T. ; Binns, K. , "Feasibility study of a multi-carrier dual-use imaging radar and communication system", Radar Conference, 2007. EuRAD 2007. European, p. 194-197, 10-12 October 2007.
6. Sturm, C. ; Inst. fur Hochfrequenztech. und Elektron., Univ. of Karlsruhe (TH), Karlsruhe; Zwick, T. ; Wiesbeck, W., "An OFDM System Concept for Joint Radar and Communications Operations", Vehicular Technology Conference, 2009. VTC Spring 2009. IEEE 69th, p. 1-5, 26-29 April 2009.
7. Neri Vela, R. Lneas de Transmisin. Ed. McGraw-Hil. Captulo 4.
8. Sandra Costanzo, Giuseppe Di Massa, David Moreno, Francesco Spadafora; "Multipurpose Software Defined Measurement System for Dielectric Characterization", The 8th European Conference on Antennas and Propagation (EuCAP 2014), The Hague; 04/2014

9. Chen, L.F.; Ong, C.K.; Neo, C.P., Varadan. Microwave Electronic Measurements and Material Characterization. Jhon Wiley and Sons. 2004. Pg. 195.
10. Varadan V. In Situ Microwave Characterization of Non Planar Dielectric Objects. IEEE Transactionson Microwave Theory. Vol 48, No 3, March 2000.
11. Ghodgaonkar, D. Vasundra, V. Varadan, V. Free Space Measurement of Complex Permittivity and Complex Permeability of Magnetic Materials at Microwave Frequencies. IEEE Transactions on Instrumentation and Measurement. Vol 39, No 2. 1990.
12. Brumbi, D. Fundamentals of Radar Technology for Level Gauging. 4 th Ed. 2003. Ed. Krhone. Chapter 7
13. Pozar, D. Microwave Theory. 3rd Ed. Jhon Wiley and Sons.
14. Chen, L.F.; Ong, C.K.; Neo, C.P., Varadan. Microwave Electronic Measurements and Material Characterization. Jhon Wiley and Sons. 2004. Pg. 299.
15. Balanis, C., Antenna Theory, Analysis and Design, John Wiley & Sons, 2005, pp. 816.
16. Cadena, J. Acero, J. Caracterizacin de Materiales Moldeables a 2.45 GHz. Universidad Nacional de Colombia 2010
17. Pozar, D. Microwave Theory. 3rd Ed. Jhon Wiley and Sons. Chapter 3.
18. www.radartutorial.eu      "Frequency-Modulated      Continuous-Wave Radar". Retrieved 2012-08-07.
19. Md Anowar Hossain, Ibrahim Elshafiey and Majeed A. S. Alkanhal (2013). "Multi-Frequency Image Fusion Based on MIMO UWB OFDM Synthetic Aperture Radar", New Advances in Image Fusion, Dr. Qiguang Miao (Ed.), ISBN: 978-953-51-1206-8, InTech, DOI: 10.5772/56943. Available from: <http://www.intechopen.com/books/new-advances-in-image-fusion/multi-frequency-image-fusion-based-on-mimo-uwb-ofdm-synthetic-aperture-radar>
20. S. Costanzo, F. Spadafora, H.O. Moreno, F. Scarcella, G. Di Massa. "Multi-band Software Defined Radar for Soil Discontinuities Detection", Journal of Electrical and Computer Engineering Volume 2013 (2013), Article ID 379832, 6 pages, <http://dx.doi.org/10.1155/2013/379832>
21. Sandra Costanzo<sup>1</sup>, Francesco Spadafora, Giuseppe Di Massa, Antonio Borgia, Antonio Costanzo, Gianluca Aloï, Pasquale Pace, Valeria Loscri, and Hugo O. Moreno. "POTENTIALITIES OF USRP-BASED SOFTWARE DEFINED RADAR SYSTEMS". Progress In Electromagnetics Research B, Vol. 53, 417435, 2013
22. Ettus, M., USRP users and develepers guide, Aug. 2006, <http://www.ettus.com/>.
23. Zhang, H., L. Li, and K. Wu, 24 GHz software-defined radar system for automotive applications, European Conference on Wireless Technologies, 138141, Munich, Germany, 2007.
24. Garmatyuk, D., J. Schuerger, and K. Kauffman, Multifunctional software-defined radar sensor and data communication system, IEEE Sensors Journal, No. 1, 99106, 2011.
25. Capria, A., M. Conti, D. Petri, M. Martorella, F. Berizzi, E. Dalle Mese, R. Soletti, and V. Carulli, Ship detection with DVB-T software defined passive radar, IEEE Gold Remote Sensing Conference, 2010.
26. Prathyusha, C., S. N. Sowmiya, S. Ramanathan, R. Soman, K. P. Amrita, V. V. Deepthi, M. Chinnam, and J. Nandhini, Implementation of a low cost synthetic aperture radar using software defined radio, International Conference



- on Computing Communication and Networking Technologies (ICCCNT), 17, 2010.
27. Ralston, J. and C. Hargrave, Software defined radar: An open source platform for prototype GPR development, IEEE International Conference on Ground Penetrating Radar (GPR), 172177, Jun. 48, 2012.
  28. Prabaswara, A., A. Munir, and A. B. Suksmono, GNU Radio based software-defined FMCW radar for weather surveillance application, International Conference on Telecommunication Systems, Services, and Applications (TSSA), 227230, Oct. 2021, 2011.
  29. Fernandes, V. N. and J. Flynn, Implementation of a radar system using Matlab and the USRP, California State University, Northridge, 2012.
  30. Braun, M., M. Muller, M. Fuhr, and F. K. Jondral, A USRP-based testbed for OFDM-based radar and communication systems, Proceedings of 22nd Virginia Tech. Symposium on Wireless Communications, Blacksburg, Jun. 2012.
  31. Robinson, L.A. ; Stanford Research Institute, Menlo Park, Calif. ; Weir, William B. ; Young, L., "Location and Recognition of Discontinuities in Dielectric Media Using Synthetic RF Pulses", Proceedings of the IEEE (Volume:62 , Issue: 1 ), p. 36-44, January 1974.
  32. Weir, William B. ; Stanford Research Institute, Menlo Park, Calif., "Automatic measurement of complex dielectric constant and permeability at microwave frequencies", Proceedings of the IEEE (Volume:62 , Issue: 1 ), p. 33-36, January 1974.
  33. Snchez M. Kerly L. "APLICACION DE RADAR DE PENETRACION DE SUELOS (GPR) PARA LA CARACTERIZACION GEOTECNICA DE SUELOS." Tutor academico: Prof. Dr. Gustavo Malav. Tutor Industrial: MSc. Miguel Gonzalez. Tesis. Caracas, U.C.V. Facultad de Ingeniera. Escuela de Geologa, Minas y Geofisica. 2004, n pag. (146). Caracas - Venezuela
  34. Prez Gracia, Mara de la Vega, "Radar de subsuelo.Evaluacion para aplicaciones en arqueologia y en patrimonio historico-artstico". Universitat Politcnica de Catalunya. Departament d'Enginyeria del Terreny, Cartogrfrica i Geofisica. 2001-10-26. Chapter 11
  35. Edel Serafn Hernandez Gmez/Jos Luis Olvera Cervantes/ Alonso Corona Chavez/Georgina Rosas Guevara. "Desarrollo de un sistema de bajo costo para el sensado de la permitividad de materiales dielctricos en el rango de microondas". SOMI Congreso de Instrumentacin. XXIX Edicin, Puerto Vallarta, Jalisco, Mexico, 10/2014
  36. Humberto Lobato-Morales, D. V. B. Murthy, Alonso Corona-Chvez, et al. Permittivity Measurements at Microwave Frequencies Using Epsilon-Near-Zero (ENZ) Tunnel Structure. IEEE transactions on microwave theory and techniques, Vol. 59, NO. 7, JULY 2011.
  37. Thomas S. Laverghetta Modern Microwave Measurement and Techniques Artech House, INC. 1988.
  38. Sandra Costanzo, Giuseppe Di Massa and Hugo Oswaldo Moreno (2012). Microwave Open Resonator Techniques Part II: Applications, Microwave Materials Characterization, Prof. Sandra Costanzo (Ed.), ISBN: 978-953-51-0848-1, InTech, DOI: 10.5772/50996. Available from: <http://www.intechopen.com/books/microwave-materials-characterization/microwave-open-resonator-techniques-part-ii-applications>

39. S. Costanzo, G. Di Massa, O. H. Moreno "EQUIVALENT IMPEDANCE RETRIEVAL OF PLANAR SURFACES BY OPEN RESONATOR TECHNIQUE". Proceedings of the XIX RiNEM
40. R. E. Collin, Foundations for Microwave Engineering, 2nd edition, IEEE Press, New York, NY, 2001.
41. Montgomery, C. G. Dicke, Robert H. Edward M. Purcell, Principles of microwave circuits / edited by C.G. Montgomery, R.H. Dicke, E.M. Purcell, Peter Peregrinus on behalf of the Institution of Electrical Engineers, London, U.K., 1987.
42. T. Wangler, RF linear accelerators, Wiley (2008)
43. O. M. Bucci, and G. Di Massa, Open resonator powered by rectangular waveguide, IEE Proc. H, vol. 139, pp. 323-329, 1992.
44. G. Di Massa, S. Costanzo, and O. H. Moreno, Accurate circuit model of open resonator system for dielectric material characterization, Journal of Electrom. Waves Applicat., vol. 26, pp. 783-794, 2012.
45. Peter Y. Yu, Manuel Cardona (2001). Fundamentals of Semiconductors: Physics and Materials Properties. Berlin: Springer. p. 261. ISBN 3-540-25470-6.
46. Jos Garca Sol, Jose Sol, Luisa Bausa, (2001). An introduction to the optical spectroscopy of inorganic solids. Wiley. Appendix A1, pp, 263. ISBN 0-470-86885-6.
47. John H. Moore, Nicholas D. Spencer (2001). Encyclopedia of chemical physics and physical chemistry. Taylor and Francis. p. 105. ISBN 0-7503-0798-6.
48. Sol, Jos Garca; Baus, Louisa E; Jaque, Daniel (2005-03-22). Sol and Bausa. p. 10. ISBN 3-540-25470-6.
49. Hartmut Haug, Stephan W. Koch (1994). Quantum Theory of the Optical and Electronic Properties of Semiconductors. World Scientific. p. 196. ISBN 981-02-1864-8.
50. Manijeh Razeghi (2006). Fundamentals of Solid State Engineering. Birkhauser. p. 383. ISBN 0-387-28152-5.
51. Nawfal Jebbor; Seddik Bri. "A microwave method for complex permittivity extraction of thin materials", Journal of Microwaves, Optoelectronics and Electromagnetic Applications vol.11 no.2 So Caetano do Sul Dec. 2012, <http://dx.doi.org/10.1590/S2179-10742012000200006>
52. Bosisio, R.G. ; Dept. de Genie Electr., Ecole Polytech., Montreal, QC, Canada ; Akyel, C. ; LaBelle, R.C. ; Wen Wang. "Computer-aided permittivity measurements of moistened and pyrolyzed materials in strong RF fields (part II)", Instrumentation and Measurement, IEEE Transactions on (Volume:IM-35 , Issue: 4 ) pp 606 - 611; December 1986
53. Nawfal Jebbor, Seddik Bri, A. M. Snchez, Mohamed Chaïbi. "Uncalibrated Microwave Measurements for Complex Permittivity Determination of Dielectric Materials at X-Band frequencies", International Journal of Microwaves Applications, Volume 1, No 1, November - December 2012, Available Online at <http://warse.org/pdfs/ijma06112012.pdf>
54. Kouji Shibata, Department of Electrical and Electric Systems, Hachinohe Institute of Technology 88-1, Aza-oubiraki, Ouaza-myō, Hachinohe, Aomori 031-8501, Japan. "Broadband Measurement of Complex Permittivity for Liquids Using the Open-ended Cut-off Circular Waveguide Reflection Method", Progress In Electromagnetics Research Symposium Proceedings, Guangzhou, China, Aug. 2528, 2014

55. "Resources, Tools and Basic Information for Engineering and Design of Technical Applications" <http://www.engineeringtoolbox.com/relative-permittivity-d1660.html>